Redox Biology 60 (2023) 102610

Contents lists available at ScienceDirect

Redox Biology

journal homepage: www.elsevier.com/locate/redox

Ginsenoside Rd promotes omentin secretion in adipose through TBK1-AMPK to improve mitochondrial biogenesis via WNT5A/Ca^{2+} pathways in heart failure

Shiyao Wan [a,1], ZeKun Cui [a,1], Lingling Wu [a,1], Fan Zhang [a], Tao Liu [a], Jingui Hu [a], Jiangwei Tian [a], Boyang Yu [a], Fuming Liu [b,***], Junping Kou [a,**], Fang Li [a,*]

[a] Jiangsu Key Laboratory of TCM Evaluation and Translational Research, Research Center for Traceability and Standardization of TCMs, School of Traditional Chinese Pharmacy, China Pharmaceutical University, Nanjing, 211198, China
[b] Jiangsu Province Hospital of Chinese Medicine, Affiliated Hospital of Nanjing University of Chinese Medicine, Nanjing, 210029, China

ARTICLE INFO

Keywords:
Ginsenoside Rd
Heart failure
Adipose-myocardium crosstalk
Omentin
WNT5A
Mitochondrial biogenesis

ABSTRACT

Ginsenoside Rd is an active ingredient in *Panax ginseng* CA Mey and can be absorbed into the adipose tissue. Adipokines play an important role in the treatment of cardiovascular diseases. However, the potential benefit of Rd on heart failure (HF) and the underlying mechanism associated with the crosstalk between adipocytes and cardiomyocytes remains to be illustrated. Here, the results identified that Rd improved cardiac function and inhibited cardiac pathological changes in transverse aortic constriction (TAC), coronary ligation (CAL) and isoproterenol (ISO)-induced HF mice. And Rd promoted the release of omentin from the adipose tissue and up-regulated omentin expression in lipopolysaccharide (LPS)-induced 3T3-L1 adipocytes. Further, Rd could increase TBK1 and AMPK phosphorylation in adipocytes. And also, the TBK1-AMPK signaling pathway regulated the expression of omentin in LPS-induced adipocytes. Moreover, the omentin mRNA expression was significantly decreased by TBK1 knockdown in LPS-induced 3T3-L1 adipocytes. Additionally, molecular docking and SPR analysis confirmed that Rd had a certain binding ability with TBK1, and co-treatment with TBK1 inhibitors or TBK1 knockdown partially abolished the effect of Rd on increasing the omentin expression and the ratio of *p*-AMPK to AMPK in adipocytes. Moreover, we found that circulating omentin level diminished in the HF patients compared with healthy subjects. Meanwhile, the adipose tissue-specific overexpression of omentin improved cardiac function, reduced myocardial infarct size and ameliorated cardiac pathological features in CAL-induced HF mice. Consistently, exogenous omentin reduced mtROS levels and restored $\Delta\psi M$ to improve oxygen and glucose deprivation (OGD)-induced cardiomyocytes injury. Further, omentin inhibited the WNT5A/Ca^{2+} signaling pathway and promoted mitochondrial biogenesis function to ameliorate myocardial ischemia injury. However, WNT5A knockdown inhibited the impairment of mitochondrial biogenesis and partially counteracted the cardioprotective effect of omentin *in vitro*. Therefore, this study indicated that Rd promoted omentin secretion from adipocytes through the TBK1-AMPK pathway to improve mitochondrial biogenesis function via WNT5A/Ca^{2+} signaling pathway to ameliorate myocardial ischemia injury, which provided a new therapeutic mechanism and potential drugs for the treatment of HF.

1. Introduction

Heart failure (HF) is a secondary syndrome caused by inadequate

* Corresponding author. Jiangsu Key Laboratory of TCM Evaluation and Translational Research, Research Center for Traceability and Standardization of TCMs, School of Traditional Chinese Pharmacy, China Pharmaceutical University, 639 Longmian Road, Nanjing, 211198, China.
** Corresponding author. Jiangsu Province Hospital of Chinese Medicine, Affiliated Hospital of Nanjing University of Chinese Medicine, Nanjing, 210029, Jiangsu, China.
*** Corresponding author.
E-mail addresses: doctor.liufuming@outlook.com (F. Liu), junpingkou@cpu.edu.cn (J. Kou), lifangcpu@163.com (F. Li).
[1] These authors contributed equally to this work.

https://doi.org/10.1016/j.redox.2023.102610
Received 3 January 2023; Accepted 10 January 2023
Available online 14 January 2023
2213-2317/© 2023 The Authors. Published by Elsevier B.V. This is an open access article under the CC BY-NC-ND license (http://creativecommons.org/licenses/by-nc-nd/4.0/).

Abbreviations

AAV	adeno-associated virus
AICAR	Acadesine;
AMPK	AMP-activated protein kinase
Amx	Amlexanox
CAL,	coronary artery ligation
Enalapril	EP
CAP	Captopril
CAMKII	Calmodulin-dependent protein
CC	Compound C
CM	conditioned medium
Dex	dexamethasone
EAT	epicardial adipose tissue
HF	heart failure
IF	Immunofluorescence Staining analysis
IHC	Immunohistochemistry analysis
ISO	isoproterenol
JC-1	5,5′,6,6′-tetrachloro-1,1′,3,3′-tetraethyl-benzimidazolylcarbocyanine iodide;
LDH	lactate dehydrogenase
IL-6	Interleukin-6
LPS	lipopolysaccharide;
LVEF	the left ventricular ejection fraction
LVFS	the left ventricular shortening fraction
IVS	d, the interventricular septum in diastole
LVID	d, the left ventricle interior diameter in diastole
LVPW	d, the left ventricle posterior wall in diastole
LV Mass corrected	the left ventricular Mass corrected
LV Vol	d, the left ventricular volume in diastole
MDA	Malondialdehyde; Met, Metoprolol
MTT	3-(4,5-dimethylthiazol-2-yl)-2,5-diphenyltetrazolium bromide;
mtROS	mitochondrial ROS
ΔψM	mitochondrial membrane potential
mtDNA	mitochondrial DNA
NRF1	nuclear respiratory factor 1
NRF2	nuclear respiratory factor 2
NT-proBNP	N-terminal pro-B type natriuretic peptide;
OGD	oxygen and glucose deprivation
PBS	phosphate-buffered formalin
p-CAMKII	phospho-CAMKII
PGC-1α	Proliferator-activated receptor-γ co-activator 1α
TNF-α,	tumor necrosis factor alpha
TAC-induced	transverse aortic constriction-induced
TBK1	TANK binding kinase 1
TFAM	mitochondrial transcription factor
WB	Western Blot Analysis

ventricular filling or ejection [1]. HF patients have suffered from high hospitalization rates and poor prognoses in the rehabilitation process for many years [2], which has brought an enormous burden to society. Therefore, it is necessary to understand the pathophysiological mechanism further and find complementary treatment strategies for HF.

In recent years, the interaction between the adipocytes and cardiomyocytes has provided new strategies to prevent and treat HF [3]. Adiponectin stimulates exosome secretion from mesenchymal stem cells to ameliorate pressure-overload HF [4]. High leptin concentrations can trigger HF by causing mitochondrial dysfunction in the myocardial cells [5]. Additionally, omentin is a novel adipokine that could attenuate acute myocardial ischemia/reperfusion injury through (AMP)-activated protein kinase (AMPK) and Akt-dependent mechanisms [6]. The activity of TANK binding kinase 1 (TBK1) was markedly up-regulated in the adipose tissue of obese mice [7], while TBK1 attenuates NF-kB activation by phosphorylation, mediates the anti-inflammatory effect of AMPK and inhibits the release of adipose inflammatory factor tumor necrosis factor-alpha (TNF-α) [8]. However, whether omentin could improve HF and the potential mechanism remain obscure. Moreover, the mechanism by which adipocytes release omentin remains to be further elucidated.

The heart is an organ with high energy requirements, which largely depends on the ability of mitochondrial biogenesis to generate energy [9]. Proliferator-activated receptor-γ co-activator 1α (PGC-1α), a member of the transcriptional coregulatory family that binds to other transcription factors, promotes biogenesis in cardiac mitochondria [10]. However, Ca^{2+} overload suppresses PGC-1α expression, mitochondrial biogenesis, and finally leads to mitochondrial dysfunction [11]. Previous research has shown that WNT5A/Ca^{2+} inhibition could inhibit apoptosis and improve HF after myocardial ischemia-reperfusion [12]. Therefore, regulating the WNT5A/Ca^{2+} signaling pathway and mitochondrial biogenesis is crucial for improving HF. The elucidation of related mechanisms may provide new therapeutic strategies to prevent and treat HF.

As an emerging medicine, ginsenosides have excellent potential in preventing and treating obesity, diabetes, cardiovascular disease and associated diseases [13]. Ginsenoside Rd is an essential component of ginsenosides and could alleviate transverse aortic constriction (TAC)--induced cardiac hypertrophy by inhibiting oxidative stress and inflammation [14]. In our previous research, Rd is one of the main components in ginseng and can be absorbed into the adipose tissue [15]. Nevertheless, it remains unclear how Rd promotes the release of omentin from adipose tissue to improve HF.

Therefore, this study mainly explored the mechanism of omentin released from adipocytes and elucidated the protective effect of omentin on HF. Meanwhile, the cardioprotective effect and potential mechanism of Rd were further clarified from the crosstalk between adipose and myocardial tissue.

2. Materials and methods

2.1. Drugs and reagents

Ginsenoside Rd ($C_{48}H_{82}O_{18}$; molecular weight, 947.166; purity ≥99%) was obtained from Pufei De Biotech Co., Ltd (Chengdu, China). Lipopolysaccharide (LPS, L2880), Captopril (CAP, C4042), isoproterenol (ISO, I5627), 3-isobutyl-1-methylxanthine (IBMX, I5879), dexamethasone (Dex, D4902) were purchased from Sigma (St. Louis, MO, USA). Insulin was purchased from Wanbang Biopharmaceuticals (Jiangsu, China). Metoprolol (Met, 1409093) was obtained from AstraZeneca Pharmaceutical (London, UK). Omentin protein was obtained from AdipoGen Life Sciences (AG-40B-0042–3010, San Diego, USA). DMEM and DMEM/F12 were obtained from GIBCO/BRL, Life Technologies (Carlsbad, CA, USA).

For western blotting analysis, the following primary antibodies were obtained from Affinity: anti-WNT5A Ab (1:1000, DF6856); anti-Frizzled2 Ab (1:1000, AF5282); anti-nuclear respiratory factor 1 Ab (NRF1; 1:1000, AF5298); anti-mitochondrial transcription factor A Ab (TFAM, 1:1000, DF3232), Anti-TBK1 Ab (1:1000, DF7026); anti-omentin Ab (1:1000, ab232885). The following primary antibodies were obtained from Proteintech: anti-PGC-1α Ab (1:1000, 66369-1-Ig); anti-nuclear respiratory factor 2 Ab (NRF2, 1:1000, 16396-1-AP). The following primary antibodies were obtained from Cell Signaling Technology: anti-phospho-CAMKII Ab (*p*-CAMKII, 1:1000, D21E4); anti-phospho-AMPK Ab (*p*-AMPK, 1:1000, 2535S); anti-AMPK Ab (1:1000, 2532S), anti-Phospho-TBK1 Ab (*p*-TBK1, 1:1000, 5483S). anti-Calmodulin-dependent protein Ab (CAMKII, 1:1000, GR124797-6) was

obtained from Abcam. Anti-β-actin Ab (1:1000, 200068-8F10) was purchased from ZenBio.

2.2. Human samples

A total of 58 heart failure (HF) patients and 38 healthy subjects were selected from the Jiangsu Province Hospital of Traditional Chinese Medicine. A clinician comprehensively evaluated the results of electrocardiography, echocardiography and BNP (HF-associated biochemical indexes) to screen out clinical HF patients. Informed consent was obtained from all human research participants and this study was guided by the Helsinki Declaration (No. 2019NL-089-02). The characteristics of heart failure patients and healthy subjects were shown in Supplementary Table 1.

2.3. Animals and treatments

All procedures followed the guidelines for the Care and Use of Laboratory Animals issued by the National Institutes of Health. The experimental protocols were in line with the Animal Ethics Committee of China Pharmaceutical University (SYXK2021-0010). The sample size of each group in the experiment was determined according to the experimental scheme of our previous study. All the animal studies were designed to produce equally sized groups using randomized and blinded analysis [16,17]. Animal studies are reported in line with the ARRIVE guidelines [18].

C57BL/6J mice (8 weeks; 23–27g) were purchased from the Experimental Animal Center of Yangzhou University (Yangzhou, China, certificate NO SYXK 2021–0011). As previously described [19], the transverse aortic constriction (TAC)-induced HF model was established. Male mice were anesthetized with isoflurane and the left chest of each mice was opened to expose the aorta of the heart. The exposed aorta was sutured with a 27-gauge needle and 6-0 silk thread. Finally, the chest cavity was sutured. The sham group underwent a similar procedure but were not ligated. The surviving mice were separated randomly into seven groups (n = 12/group): the sham operation group, the TAC group (TAC 28 d), the ginsenoside Rd group (TAC 28 d, 5 mg/kg, 10 mg/kg, 20 mg/kg, i.g.), the Enalapril (EP) group (TAC 28 d, 2.6 mg/kg, i.g.) and the sham with ginsenoside Rd group. EP is a positive drug. Mice undergoing sham operation were intraperitoneally injected with normal saline. According to the difference in each group, maintenance therapy was given for four weeks (once a day). Cardiac function was then assessed with an echocardiogram.

ICR male mice (8 weeks old; 23–27 g) were purchased from the Experimental Animal Center of Yangzhou University (Yangzhou, China, certificate NO SYXK 2021–0011). As previously described [20], the coronary artery ligation (CAL)-induced HF model was established. The left anterior descending coronary artery was ligated in mice in simple terms. After that, the surviving mice were divided randomly into model groups and administration groups. The sham group underwent the same procedure without ligation of the anterior descending branch of the left coronary artery. Mice were anesthetized with isoflurane. Each group of mice was blindly assigned, and the animals survived more than 90% after surgery. The surviving mice were separated randomly into seven groups (n = 12/group): the sham operation group, the CAL group (CAL 14 d), the ginsenoside Rd group (CAL 14 d, 5 mg/kg, 10 mg/kg, 20 mg/kg, i.g.), the CAP group (CAL 14 d, 0.16 g/kg, i.g.) and the sham with ginsenoside Rd group. CAP is a positive drug. Mice undergoing sham operation were intraperitoneally injected with normal saline. According to the difference in each group, maintenance therapy was given for two weeks (once a day).

Meanwhile, the isoproterenol (ISO)-induced HF model was also established *in vivo*. The initial damage treatment was given ISO (5 mg/kg, i.g.) once a day for three weeks. The ginsenoside Rd was given once a day for the last week. The ICR mice were randomly divided into six groups (n = 12/group): the sham group, the ISO group (ISO 21 d), the ginsenoside Rd group (ISO 21 d, 5 mg/kg, 10 mg/kg, 20 mg/kg, i.g.), Met group (ISO 21 d, 5.14 mg/kg, i.g.). Met is a positive drug.

All animals were kept in temperature-controlled (23 ± 2 °C) cages with light/dark cycles for 12 h. Food and water were provided at will. At the end of the observation period, the mice were euthanized with excess carbon dioxide and hearts were removed for biochemical and histopathological examination. The collected serum was immediately stored at −70 °C for analysis.

2.4. Construction and infection of recombinant human AAV-omentin

ICR male mice (22–24 g) were purchased from the Yangzhou University (Jiangsu, China, certificate NO. 202012586). The animals were housed in a standard space with enough food and water. The adipose-specific promoters PTKAA carrying human omentin (AAV-omentin) (24538) or negative control (AAV-NC) (24537GO-AAV) were produced by Genomeditech company (Shanghai, China). AAV-omentin or AAV-NC ($2E*10^{11}$ vg/mice) were administered via direct injection in the tail vein in mice at four weeks old. Two weeks later, the infected mice underwent sham surgery and CAL surgery. Mice were randomized into four groups (n = 12/group): (i) sham group (AAV-NC, $2E*10^{11}$ vg/mice, i.v.); (ii) model group (AAV-NC, $2E*10^{11}$ vg/mice, i.v.); (iii) model + omentin group (AAV-omentin, $2E*10^{11}$ vg/mice, i.v.); (iv) sham + omentin group (AAV-omentin, $2E*10^{11}$ vg/mice, i.v.). All AAV were intravenously injected into mice two weeks before CAL. And the mice were euthanized with overdose of carbon dioxide, then heart tissues were collected two weeks after CAL. Immunohistochemistry was used to evaluate the efficiency of AAV transduction *in vivo*.

2.5. Cell culture and differentiation

Rat H9c2 myocardial cell line (RRID: CVCL_0286) was cultured in DMEM supplemented with 10% FBS, 100 U/mL penicillin, and 100 μg/mL streptomycin. The humidified atmosphere is at 37 °C, with 5% CO_2 and 95% air. In this study, oxygen and glucose deprivation (OGD) injury was conducted when cells were incubated with non-glucose DMEM for 12 h in an N_2/CO_2 incubator humidified at 37 °C in a hypoxic environment containing 94% N_2, 5% CO_2 and 1% O_2. H9c2 cells were administrated with omentin.

The mouse 3T3-L1 preadipocytes (RRID: CVCL_0123) were cultured in DMEM containing 10% FBS, 100 U/mL penicillin and 100 μg/mL streptomycin. The cultural environment was 37 °C with 5% CO_2. The cells were confluent and differentiated 48 h later. Firstly, the medium was supplemented with 1 μM insulin, 0.5 mM IBMX and 0.5 μg/mL Dex for 2 days. After the cells were cultured in medium containing 1 μM insulin for 2 days, the cells were cultured in a standard medium until 80% lipid droplets appeared. Adipose inflammation was induced by 1 μg/mL LPS for 24 h.

2.6. Primary neonatal rat ventricular myocytes (NRVMs) isolation and culture

According to the previous reports [21], neonatal rat ventricular myocytes were derived from 3 to 4 days old rats. The myocardial tissue of the left ventricular of the heart was enzymatically hydrolyzed with type II collagenase, and the myocardial cells were collected and cultured in an incubator at 37 °C, 10% FBS, and 5% CO_2. When 98% of cardiomyocytes contracted at the same frequency under a microscope, they could be used for the following experiments.

2.7. siRNA transfection

H9c2 cells were plated in six-well plates and transiently transfected with 20 nM WNT5A specific small-interfering RNA (siRNA) obtained from Genesyntech Biotech (CT0002 Nantong Jiangsu, China) using Transfection Reagent according to the manufacturer's instructions.

Total cell lysates were determined by western blotting to assess the WNT5A siRNA efficiency. Rat-WNT5A-si (Sense:5′-AACCUGGCAGAUGU-3'; Antisense:5′-ACAUCUGCCAGGUUGUA.

UACUGUCC-3′); Rat-WNT5A-NC (Sense:5′-UUCUCCGAACGUGUCACGUdTdT-3'; Antisense: 5′-ACGUGACACGUUCGGAGAADTDT-3′). In addition, control siRNA and mouse TBK1 siRNA were purchased from Santa Cruz Biotechnology (sc-37007, sc-39059). Transfection with siRNA was performed using Lipofectamine RNAiMAX reagent and Opti-MEM according to the manufacturer's instructions. Following adipocyte differentiation, starting on day2, 3T3-L1 cells were incubated with 50 nM of each siRNA in maturation medium and cultured until day 5.

2.8. Echocardiographic measurement

After 14 days of treatment, according to the previous study [22], cardiac function and dimensions were measured by the Vevo 3100LT system (Visual Sonics, Toronto, Canada). These parameters included the left ventricular ejection fraction (LVEF), the left ventricular shortening fraction (LVFS), the interventricular septum in diastole (IVS; d), the left ventricle interior diameter in diastole (LVID; d), the left ventricle posterior wall in diastole (LVPW; d), the left ventricular mass corrected (LV Mass corrected), the left ventricular volume in diastole (LV Vol; d), stroke volume (SV) and relative wall thickness (RWT). Based on the measurements, the following parameters were calculated as cardiac function indicators: left ventricular fractional shortening (LV FS) = (LVID d - LVIDs)/LVID d; left ventricular ejection fraction (LV EF) = (LVEDV - LVESV)/LVEDV; stroke volume (SV) = (LV Vold - LV Vols). The following parameters were calculated as cardiac hypertrophy indicators: left ventricular mass (LV Mass) = $1.053 \times [(\text{LV Vold} + \text{LVPWd} + \text{IVSd})^3 - \text{LV Vold}^3]$; relative wall thickness (RWT) = $2 \times$ (LVPWd/LVIDd) [23].

2.9. Histological analysis

The heart was immersed in 10% formalin and fixed for 48 h, then paraffin-embedded and cut into slices of 4–5 μm. The tissue was then stained with hematoxylin-eosin and Masson trichrome, and finally photographed under a light microscope (DX45, Olympus Microsystems Ltd., Japan).

2.10. TTC staining

The hearts were rapidly removed and perfused with PBS, and then cut into five slices perpendicular to the long axis of the heart. The slices of hearts were incubated in 1% 2,3,5-triphenyl tetrazolium chloride (TTC, Macklin, Shanghai, China) solution at 37 °C for 15 min, and pictured timely. The red area of the heart stained by TTC represented viable tissue, and the negative staining areas represented infarcted myocardium. The infarct areas were analyzed through Image J software (Bethesda Md, USA).

2.11. DiOH-BDP imaging detection

Photoacoustic imaging of mice was performed using the Vevo 2100 LAZR PA Imaging System. The frequency of the photoacoustic system is 21 MHz and the acquisition frequency is five frames/s. 100 μM DiOH-BDP (150 μL) was injected intravenously into the mice 5 h before the experiment. The mice were anesthetized with 3% isoflurane, and the mice were fixed on the operating table with tape. The isoflurane concentration was maintained at 1.5% during the experiment, and the respiratory rate of the mice was 70–80 bpm. A transducer with a wavelength of 770 nm was used to collect signals in the experiment.

2.12. Serum biochemical indicators and omentin determination

After the observation, blood samples were collected from mice and serum were separated. According to the instructions, the contents of N-terminal pro-B type natriuretic peptide (NT-proBNP, HB533-Mu, Hengyuan, Shanghai, China), malondialdehyde (MDA, A003-1-2, Jiancheng, Nanjing, China), lactate dehydrogenase (LDH, A020-2-2, Hengyuan, Shanghai, China) and omentin (HB310-Mu, Hengyuan, Shanghai, China) were determined by ELISA kit. Adipokines released by 3T3-L1 adipocytes were detected by TNF-α (HB049-Mu, Hengyuan, Shanghai, China) Elisa kits.

2.13. Adipose tissue-derived conditioned medium (CM) preparation

The epicardial adipose tissue (EAT) was separated from the heart and cut into small pieces. The same amount of EAT was cultured in fresh DMEM from mice with the sham group, CAL group, ginsenoside Rd (5 mg/kg, 10 mg/kg, 20 mg/kg), and captopril group (0.16 g/kg). The medium was collected as CM after 24 h.

2.14. Cell viability and LDH detection

Cell viability was detected by 3-(4,5-dimethylthiazol-2-yl)-2,5-diphenyltetrazolium bromide (MTT, Amresco, Washington, USA) assay. H9c2 cells were plated into 96-well microtiter plates at a density of 6×10^3 cells/well. After different treatments, MTT solution (5 mg/mL) was added into the cells and incubated for 4 h, then DMSO was added to dissolve formazan. Finally, the absorbance was read at 570 nm and the reference wavelength was 650 nm. In addition, the release of LDH was measured to evaluate the degree of cell injury. After the incubation period, the culture supernatants of H9c2 cells were collected to detect the activity of LDH at 490 nm.

2.15. Western Blot analysis (WB)

The protein concentration was calculated using a BCA protein assay kit (P0012, Beyotime, Shanghai, China) following the manufacturer's instructions [24]. Equal amounts of total protein (40 μg) were electrophoresed on 10% SDS-PAGE gels and transferred onto PVDF membranes. The membranes were then blocked with 5% BSA and incubated overnight at 4 °C with specific primary antibodies.

The blots were probed with a peroxidase-conjugated secondary antibody (dilution 1:10000, Bioworld, Louis Park, MN, USA). The protein-antibody complexes were subsequently detected with ECL plus system (Vazyme, Nanjing, China), visualized by ChemiDoc™ MP System (Bio-Rad) and analyzed using Image Lab™ Software (version 4.1, Bio-Rad).

2.16. Immunofluorescence staining analysis (IF)

After modeling, mature adipocytes 3T3-L1 were washed with cold PBS for three times, fixed with 4% paraformaldehyde, sealed with 5% BSA, and incubated with primary antibody (diluted 1:300) at 4 °C overnight. After being washed three times with cold PBS, the cells were incubated with a secondary antibody (diluted 1:300, Bioworld, Technology, Louis Park, MN, USA) for 2 h. Finally, the nuclei were stained with DAPI and the fluorescence intensity was measured under a confocal laser scanning microscope (LSM700, Zeiss, Jena, Germany).

2.17. Immunohistochemistry analysis (IHC)

The inguinal fat of mice was fixed with 4% paraformaldehyde, embedded in paraffin and cut into 4 μm thickness. After dewaxing and rehydration, the inguinal fat was incubated with 3% hydrogen peroxide to block endogenous peroxidase activity. Sections were incubated in blocking liquid at 37 °C for 1 h (Beyotime, Shanghai, China) and then treated with omentin primary antibody (diluted 1:200) at 4 °C for 24 h. After washing, the slices were incubated at 37 °C for 1 h with an enzyme-conjugated secondary antibody (diluted 1:200). DAB was incubated, and

then hematoxylin was used for re-staining. Finally, immunohistochemical sections were observed under the light microscope, and images were obtained at 200× magnification.

2.18. Transmission electron microscopy

To observe the mitochondrial morphology of cardiomyocytes, fresh hearts were quickly fixed with electron microscope fixative solution at 4 °C for 2–4 h. After washing with PBS, the hearts were fixed in 1% osmic acid at room temperature, dehydrated in a gradient manner for 2 h, embedded in tissue sections, stained with 3% uranyl acetate and soaked in lead citrate for 15 min. Image acquisition and analysis were performed using a transmission electron microscope (HT7800, Hitachi Ltd, Tokyo, Japan). Mitochondrial number and bulk density were determined using image J software.

2.19. Measurement of mitochondrial ROS (mtROS) level

MtROS production was assessed by Mito SOX staining. The cells were washed with PBS after modeling. Cells were incubated in 5 μM Mito SOX Red solution (LX3608, Warbio, Nanjing, China) at 37 °C for 10 min. The red fluorescence of cells was observed by fluorescence microscope after washing with PBS for 3 times. (Ex/Em = 510 nm/580 nm).

2.20. Measurement of mitochondrial membrane potential ($\Delta\psi M$)

After treatment, cells in each group were washed with PBS twice after discarding the culture medium. The cell culture medium was mixed 1:1 with 5,50,6,60-tetrachloro-1,10,3,30-tetraethylbenzimidazolcarbocyanine iodide (JC-1) (1X) staining solution (C2006, Beyotime, Shanghai, China) for cell culture. After 20 min of incubation at 37 °C, the cell culture medium was washed twice with a cold JC-1 (1X) culture medium, and the normal medium was added at last. The immediate observation was performed with confocal laser microscopy. Image J software was used to calculate the red/green fluorescence intensity ratio (%), and the calculated value was relative to the control group. (For JC-1 green, Ex/Em = 514nm/529 nm; for JC-1 red, Ex/Em = 585 nm/590 nm).

2.21. Cytoplasmic Ca^{2+} concentration detection

The intracellular Ca^{2+} concentration was detected by Fluo-4 AM Assay Kit (S1060, Beyotime, Shanghai, China). The cells were washed with cold PBS for 3 times and incubated with Flou-4 AM (5 μM) at 37 °C for 30 min. After being washed with ice PBS for 3 times, the cells were incubated with PBS suspension at 37 °C for 20 min. Finally, the cytoplasmic Ca^{2+} content was observed under fluorescence microscope (Ex/Em = 488 nm/520 nm).

2.22. Mitochondrial permeability transition pore (MPTP) opening detection

The sensitivity of MPTP opening to Ca^{2+} was determined using the Mitochondrial Permeability Transition Pore Assay Kit (C2009S, Beyotime, Shanghai, China.), according to the manufacturer's protocol. The culture medium was poured off, washed three times with PBS, and the residue was absorbed. 200 μL of 1 × Calcein AM dye solution was added and stained for 30 min in an incubator at 37 °C. After that, when the dye solution was absorbed, it was washed three times with PBS and then 200 μL of DMEM was added for observation under a microscope (Ex/Em = 494 nm/517 nm).

2.23. Oxygen consumption rate (OCR) and extracellular acidification rate (ECAR) detection

The mitochondrial oxygen consumption (OCR) and extracellular acidification rate (ECAR) were measured by SeaHorse XF96 extracellular flux analyzer. According to the manufacturer's instructions, the cells were inoculated into the cell plate with the number of 1×10^4 cells per well, and the probe plate was hydrated at 37 °C in a non-CO_2 incubator overnight. For the assessment of mitochondrial oxygen consumption, we used continuous injection of oligomycin (final concentration: 1 μM), FCCP (final concentration: 3 μM) and rotenone/antibiotic A (final concentration: 0.5 μM). For the determination of extracellular acidification rate, we used continuous injection of glucose (final concentration: 10 mM), oligomycin (final concentration: 1 μM) and 2-DG (final concentration: 50 mM). The basic value shall be measured 3 times before dosing, and then 3 times after each dosing.

H9c2 cells were inoculated into hippocampal XF96 cell culture microplates (Agilent Technologies, USA) and treated with the specified reagents after the cells were modeled and administrated. Before measuring OCR, cells were given glucose (10 mM), pyruvate (1 mM), and L-glutamine (1 mM) -supplemented XF basal medium with minimal DMEM in 37 °C for 1 h in a CO_2 free incubator. OCR was measured at XF calibration using the Seahorse XFe96 extracellular flux assay kit (103020–100, Agilent Technologies, USA), followed by 2.5 μM oligomycin, 1 μM FCCP, and 0.5 μM rotenone/antimycin A supplementation at the appropriate port of the injection plate. To detect ECAR, cells were incubated with L-glutamine (1 mM) and XF base medium with trace DMEM. The injection plate was added with 10 mM glucose, 1 μM oligomycin and 50 mM 2-DG. OCR and ECAR were measured on a haima XFe96 analyzer (Agilent Technologies, USA) and analyzed with Wave 2.6.1 software.

2.24. ATP synthesis detection

Intracellular ATP levels were detected by an ATP detection kit (S0027, Beyotime, Shanghai, China). After modeling, the cells in each group were collected by digestion centrifugation and lysed with 200 μL lysis buffer. The cells were centrifuged at 12000 RPM at 4 °C for 5 min, and the supernatant was collected. Then, 20 μL supernatant and 100 μL ATP working solution were added to the 96-well opaque plate and analyzed by fluorescence microplate (Tecan, Infinite M200 Pro).

2.25. Quantification of mitochondrial DNA (mtDNA)

MtDNA damage of H9c2 cells was analyzed by quantitative PCR. In brief, total DNA was extracted using FastPure®Cell/Tissue DNA Isolation Mini Kit (DC102, Vazyme, Nanjing, China). According to the manufacturer's protocol, real-time PCR was performed on the Mastercycler EP Realplex PCR system (Bio-Rad). The relative expression of mtDNA was normalized by β-globin, which was assessed in separate test tubes to quantify target genes. The primers used in this study are listed in Table S2.

2.26. Mitochondrial content detection

The mitochondrial content of H9c2 cardiomyocytes was stained with Mito-Tracker Green (C1048, Beyotime, Shanghai, China). After modeling, the cells were washed with PBS for three times and incubated with 100 nM Mito-Tracker Green at 37 °C for 30 min. Then the cells were washed with PBS twice and photographed with fluorescence microscope and Image J software for analysis.

2.27. RNA isolation and quantitative real-time PCR

Total RNA was isolated from adipocytes 3T3-L1 using TRIZOL reagent (R401-01, Vazyme, Nanjing, China). HiScript®Q RT SuperMix (R223, Vazyme, Nanjing, China) was used to transcribe RNA and ChamQTM SYBR®qPCR (Q331-02, Vazyme, Nanjing, China) Master Mix for Quantitative Real-time PCR. Fusion curve analysis confirmed the specificity of PCR products [25]. Relative quantification of gene

expression was performed using the $2^{-\Delta\Delta CT}$ method. All samples were 5 copies. Gene expression was normalized to β-actin and assessed in separate test tubes to allow quantification of target genes. The primers used in this study are listed in Supplement Table 2.

2.28. Molecular docking technology

Molecular docking was performed according to the previous experimental method [26]. The 3D structure of protein TBK1 (6NT9) was downloaded from the RCSB PDB database (https://www.rcsb.org/). The two-dimensional structure of molecular ligands was downloaded from the PubChem database (https://pubchem.ncbi.nlm.nih.gov/). The receptor protein was then dehydrated and modified with PyMOL 2.4.0 software. Autodock software was used to calculate the hydrogen bond and charge of the protein. The parameters of the receptor protein's docking site included the active pocket site for the binding of small-molecule ligands. Finally, the TBK1 receptor protein with the small molecule ligand of ginsenoside Rd were docked by Autodock Vina.

2.29. Surface plasmon resonance (SPR) analysis

The affinity between TBK1 and ginsenoside Rd was analyzed using the Biacore T200 system. Soluble proteins were used as immobilized ligands diluted in 10 mM sodium acetate buffer with pH 4.0. TBK1 protein (OriGene, Maryland, USA) was immobilized on the sensor chip (CM5, GE Healthcare) using the amine-coupling method according to standard protocols. The amount of ligand immobilization was approximately 11000 RU. A similar procedure was performed with reference, but without ligand injection. Subsequently, 1.05 × PBS-P with 5% DMSO solution was used as the running buffer, and ginsenoside Rd with different concentrations was used as the analyte. For binding studies, analytes were applied at corresponding concentrations in flow buffer at a flow rate of 30 μL/min with a contact time of 60 s and a dissociation time of 120 s. The chip platform was washed with flow buffer and 50% dimethyl sulfoxide after each analysis. Biacore T200 evaluation software was performed to analyze the data through curve fitting of a 1:1 binding model.

2.30. Dual-luciferase reporter assay

The promoter activity was determined by the dual-luciferase reporter assay kit. The DNA fragment of human omentin promoter region (501 bp) was obtained by chemical synthesis, and then was inserted into the basic reporter vector pGL3. The human omentin promoter reporter vector was correctly constructed, and named as pGL3-omentin. HEK293T cells were seeded at a density of 1×10^4 cells/well in 96-well plates and grown in an incubator at 37 °C with 5% CO_2 for 24 h. And then the cells were co-transfected with pGL3-omentin and pRL-TK plasmid using Lipofectamine 2000 (Invitrogen, Carlsbad, USA). At 12 h post-transfection, ginsenoside Rd was added to the cells and incubated for 24 h. Luciferase activity was measured from lysates using luciferase assay system (Beyotime Biotech, China) in a Berthold TriStar2 SLB929 modular monochromator multimode reader (Berthold Technologies, Germany).

2.31. Statistical analysis

The statistical analyses were performed using GraphPad Prism 8 software (RRID: SCR_002798, San Diego, CA, USA) and values were expressed as mean ± SD. Student's two-tailed *t*-test and one-way analysis of variance (ANOVA) followed by the Dunnett's post hoc test were used to compare between two groups and among three or more groups respectively. All experiments were randomized and blinded, and $p < 0.05$ was considered statistically significant.

3. Results

3.1. Ginsenoside Rd ameliorated myocardial injury in HF mice

Firstly, we investigated the cardiac function of mice by echocardiography to evaluate the protective effect of ginsenoside Rd on CAL, ISO and TAC-induced HF mice (Fig. 1A, Fig. S1A and Fig. S2A). LVEF and LVFS are the most frequently-used clinical parameters to measure myocardial contractility. Rd could significantly increase the LVEF and LVFS compared with the model group (Fig. 1B–C, Figs. S1B–C and Figs. S2B–C). Meanwhile, IVS; d, LVID; d, LVPW; d, LV Mass and LV Vol; d were significantly decreased after being treated with Rd (Fig. 1D–H, Figs. S1D–H and Fig. S2 D-E). Based on the above results, Rd could improve the contractile capability and inhibit the hypertrophy in CAL, ISO and TAC-induced HF mice.

To further evaluate CAL, ISO and TAC-induced myocardial injury, the content of MDA, LDH and NT-proBNP were measured in serum. And we found that Rd could significantly decrease MDA content in CAL and TAC-induced HF mice and decrease the LDH content in ISO-induced HF mice (Fig. 1I, Fig. S2F and Fig. S1I). In addition, the level of NT-proBNP, an indicator of cardiac function in serum, was significantly elevated in the model group, while it was significantly blocked after treated with Rd (Fig. 1J, Fig. S1J and Fig. S2G). Moreover, H&E staining and Masson's trichrome staining of the heart also demonstrated the protective effects of Rd on myocardial injury. The heart tissue of mice in the model group showed prominent tissue fibrosis and collagen deposition, while Rd could prevent the occurrence of these injuries (Fig. 1K, Fig. S1K and Fig. S2H). Meanwhile, Rd could decrease the PA_{770} average threshold of the heart in TAC-induced HF mice (Fig. S2I). Collectively, Rd treatment significantly ameliorated myocardial injury in CAL, ISO and TAC-induced HF mice.

3.2. Ginsenoside Rd promoted omentin release from adipose tissue and up-regulated the omentin expression in LPS-induced 3T3-L1 adipocytes

Firstly, multiple adipokines associated with heart failure were screened and the results showed that ginsenoside Rd exerted the most obvious effect on promoting omentin release in adipocytes (Fig. S3). As an adipokine, omentin also plays an essential role in treating cardiovascular diseases. To further verify the role of Rd on the secretion of omentin in adipose tissue, the serum omentin level of mice was detected by the Elisa kit. As shown in Fig. 2A, the level of serum omentin in the CAL group was significantly reduced but gradually recovered after Rd treatment. Consistently, Rd reversed the inhibitory effect of ISO and TAC-induced HF on omentin secretion (Fig. S4). Then the CM of isolated EAT was prepared and cultured *in vitro* for 24 h. Intriguingly, omentin content was significantly elevated in the medium of EAT from Rd-treated mice compared with those of CAL-induced HF mice (Fig. 2B), supporting that Rd promoted the omentin released from EAT directly. Then, different groups of CM were used to culture H9c2 cells, respectively. Exposure of cardiomyocytes to OGD decreased cell viability, while CM (isolated EAT from Rd- and CAP-treated mice) maintained cell viability (Fig. 2C). Furthermore, LPS induced 3T3-L1 adipocyte inflammation model was established *in vitro*. The results found that 1 μg/mL LPS could significantly promote TNF-α release from 3T3-L1 adipocytes after 24 h (Fig. S5). Meanwhile, LPS suppressed the expression of omentin, while it was reversed by Rd, which was assessed by both immunofluorescence (Fig. 2D) and Western blot (Fig. 2E) analysis. Furthermore, we constructed the omentin promoter coupled to a luciferase reporter gene, to determine if Rd had effects. HEK293T cells were transfected with the omentin promoter/enhancer-Luc in the presence or absence of Rd. And we found that luciferase activity of omentin was increased upon the treatment with Rd (Fig. 2F). These results proved that Rd could promote the release of omentin from adipocytes and might have a protective effect on OGD-induced cardiomyocytes injury.

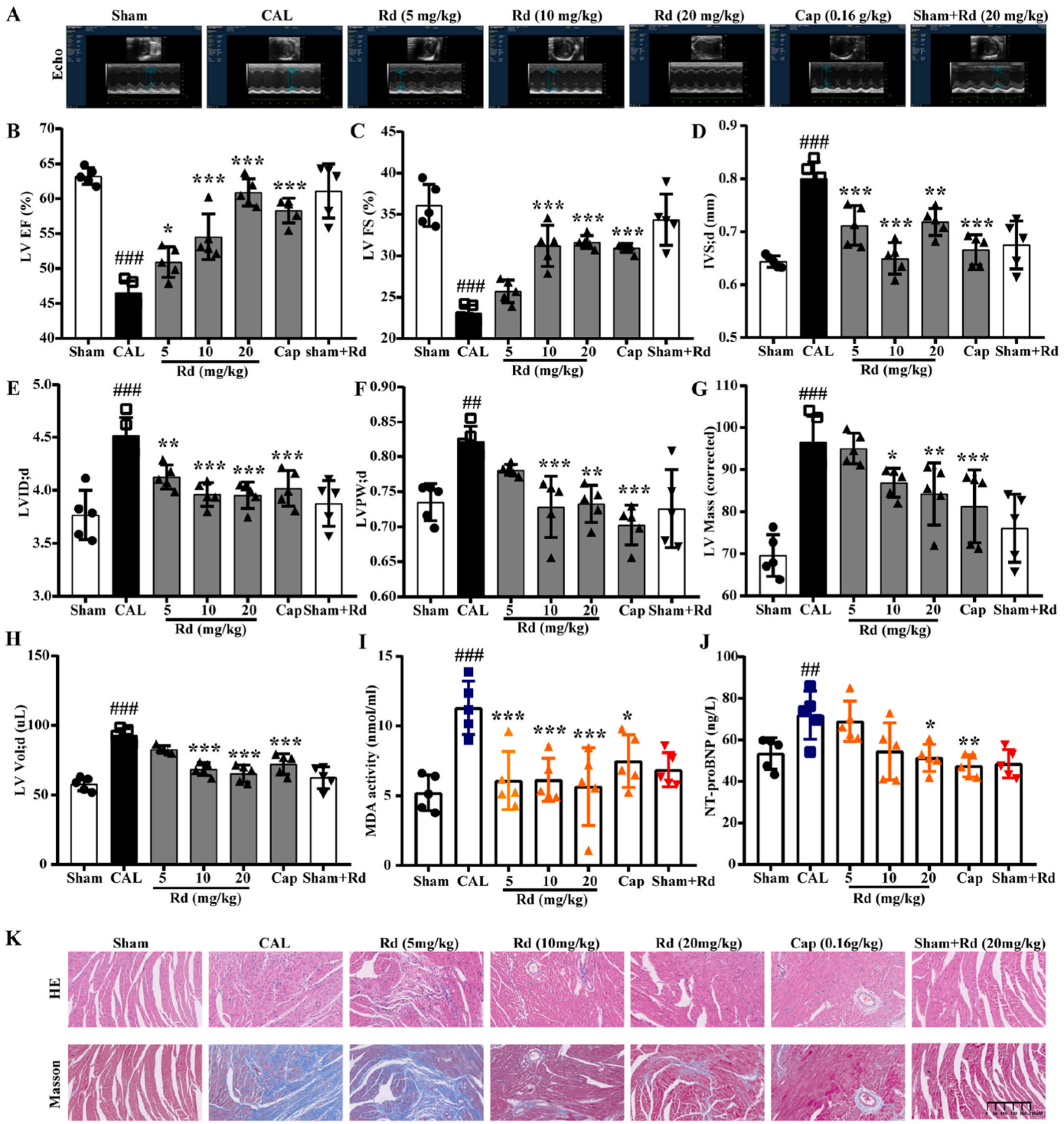

Fig. 1. Ginsenoside Rd ameliorated myocardial injury in CAL-induced HF mice. The mice were divided into seven groups randomly. The CAL group, ginsenoside Rd group and Captopril group were performed to CAL and treated with NS, ginsenoside Rd (5 mg/kg, 10 mg/kg, 20 mg/kg) and Captopril (0.16 g/kg), respectively. The sham group was treated with NS. (A) Representative M-mode echocardiograms. (B) The effect of ginsenoside Rd on LV EF, (C) LV FS, (D) IVS; d, (E) LVID; d, (F) LVPW; d, (G) LV Mass, (H) LV Vol; d changes in CAL performed mice evaluated by echocardiographic (n = 5). The MDA content (I) and NT-proBNP levels (J) in serum were detected by Elisa (n = 5). (K) Profiles of heart tissues in mice treated with ginsenoside Rd (HE staining and Masson staining) (n = 3). Values are expressed as the means ± SD. One-way ANOVA followed by the Dunnett's post hoc test was used for statistical analysis. $^{\#\#}P < 0.01$, $^{\#\#\#}P < 0.001$ vs. Sham; $^{*}P < 0.05$, $^{**}P < 0.01$, $^{***}P < 0.001$ vs. CAL. Cap = Captopril.

3.3. TBK1-AMPK signaling pathway modulated the omentin expression in LPS-induced 3T3-L1 adipocytes

AMPK is a cellular energy regulator that plays a vital role in lipid metabolism and anti-inflammatory processes, and activation of AMPK promotes adipokine production such as adiponectin and inhibits inflammatory kine synthesis. In addition, previous studies found that the TBK1-AMPK signaling pathway played a specific role in treating adipose inflammation. In our present study, we found that Rd could increase AMPK and TBK1 by enhancing phosphorylation in LPS-induced

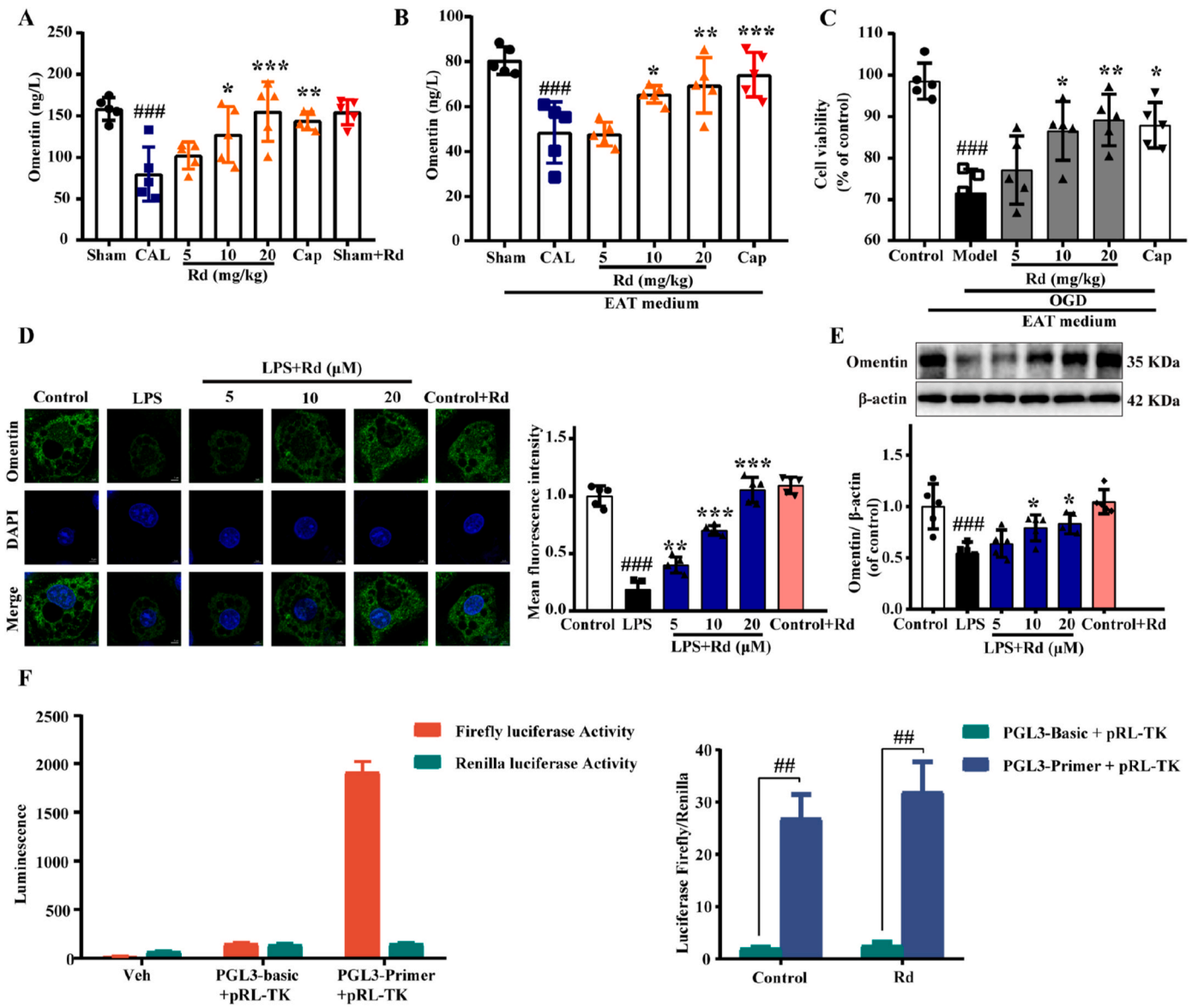

Fig. 2. Ginsenoside Rd promoted omentin release from adipose tissue and up-regulated the expression of omentin in LPS-induced 3T3-L1 adipocytes. (A) The effect of ginsenoside Rd on omentin content in serum (n = 5). (B) The omentin content in EAT medium from each group was detected by Elisa Kit (n = 5). (C) The effect of the conditioned medium on OGD-induced cardiomyocytes viability was detected by MTT (n = 5). (D) The expression of omentin in 3T3-L1 adipocytes was performed by immunofluorescence staining. Scale bar = 20 μm (n = 5). (E) The protein expression level of omentin was determined by Western blot. β-actin was used as a loading control (n = 5). (F) Omentin luciferase activity with and without Rd treatment. Values are expressed as the means ± SD. One-way ANOVA was followed by the Dunnett's post hoc test. $^{###}P < 0.001$, $^{##}P < 0.01$ vs. Sham or Control; $^{*}P < 0.05$, $^{**}P < 0.01$, $^{***}P < 0.001$ vs. CAL or LPS.

adipocytes (Fig. 3A and B). Then, we examined the mRNA expression of adipokine in 3T3-L1 mature adipocytes to investigate whether AMPK agonists affect inflammatory responses. Acadesine (AICAR) is an agonist of AMPK. As shown in Fig. 3C and D, the level of the TNF-α mRNA was significantly increased in the LPS-treated group. However, this up-regulation was alleviated by AICAR. AICAR also significantly increased the omentin mRNA expression. Consistently, the immunofluorescence staining and WB results showed that the omentin protein level was prominently reversed by AICAR treatment in LPS-treated adipocytes (Fig. 3E–F and Fig. S6A). The results indicated that the AMPK agonist effectively protected adipocytes from LPS-induced inflammatory injury and promoted the expression of omentin. In addition, compound C (CC), an AMPK inhibitor, further promoted inflammatory injury of adipocytes and inhibited the omentin mRNA expression (Fig. 3G and H). And the omentin protein level and fluorescence intensity were lower than LPS-treated adipocytes after co-treatment with CC (Fig. 3I–J and Fig. S6B). In a word, AMPK agonists and inhibitors regulated omentin expression in 3T3-L1 adipocytes. To further clarify the role of TBK1-AMPK signaling pathway in the regulation of omentin release, the TBK1 inhibitor amlexanox was conducted. As shown in Fig. 3K, treatment with TBK1 inhibitor further stimulated the mRNA expression of TNF-α. And the omentin mRNA expression, the omentin protein level and fluorescence intensity were vastly decreased by amlexanox treatment in LPS-treated adipocytes (Fig. 3L-N and Fig. S6C), which indicated that TBK1 was possibly involved in the regulation of adipose inflammation. Meanwhile, LPS inhibited phosphorylation of AMPK and it was further attenuated after treatment with amlexanox in LPS-treated adipocytes (Fig. 3O). Additionally, TBK1 siRNA was transfected into differentiated 3T3-L1 cells and we found that omentin mRNA expression was significantly decreased by TBK1 knockdown in LPS-treated adipocytes (Fig. 3P). All above results indicated that the TBK1-AMPK signaling pathway was involved in the regulation of omentin expression in LPS-

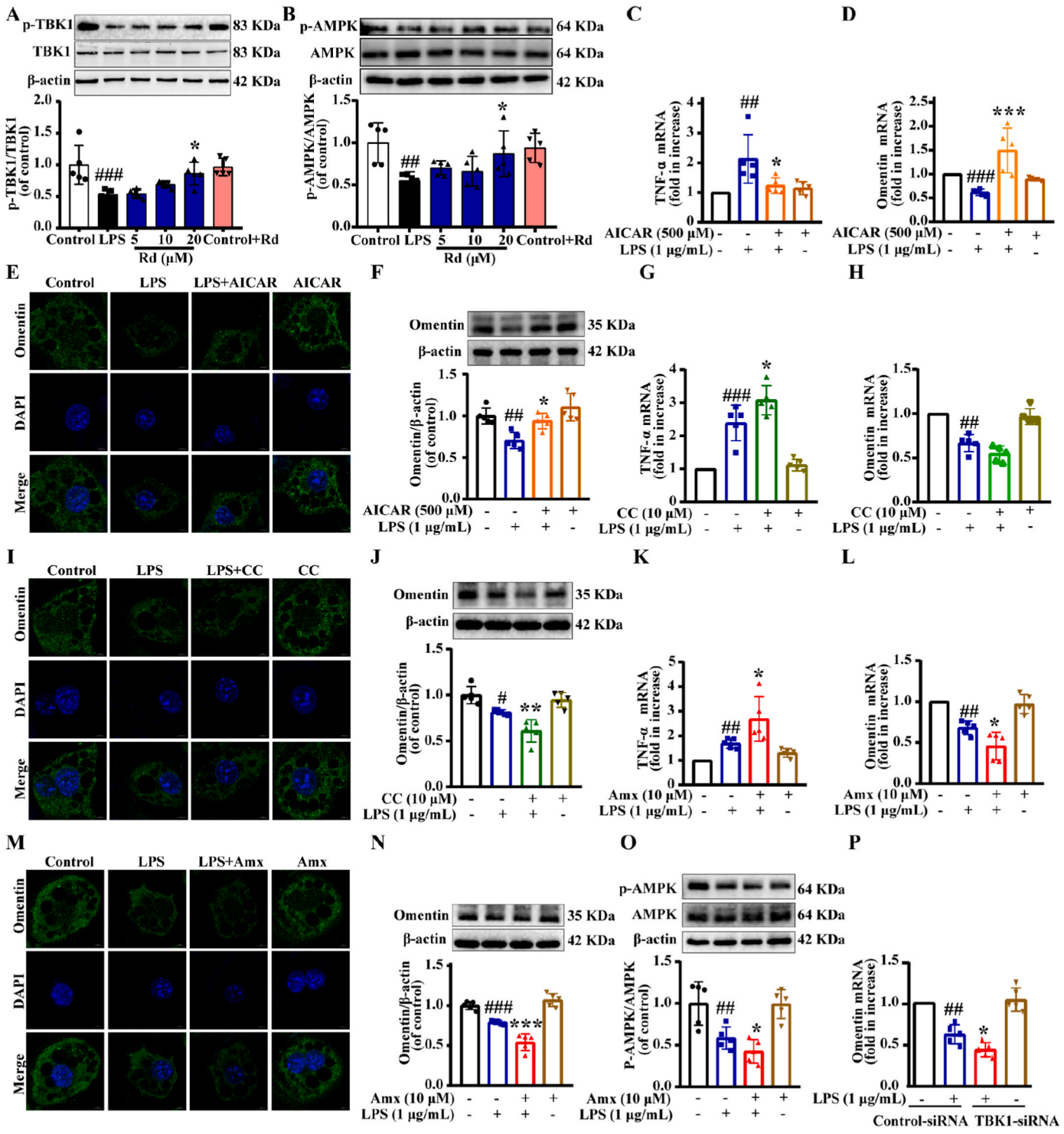

Fig. 3. TBK1-AMPK signaling pathway modulated the omentin expression in LPS-induced 3T3-L1 adipocytes. Differentiated 3T3-L1 cells were treated with or without AICAR (500 μM) for 2 h, followed by stimulation with LPS (1 μg/mL) for 24 h. (A) Expression of the ratio of *p*-TBK1 to TBK1 was measured by Western blot in differentiated 3T3-L1 cells (n = 5). (B) Expression of the ratio of *p*-AMPK to AMPK was measured by Western blot in differentiated 3T3-L1 cells (n = 5). Quantitative real-time PCR analysis of (C) TNF-α and (D) omentin mRNA expression. (E) The omentin fluorescence intensity was detected by immunofluorescence (Scale bar = 20 μm) and (F) the expression of omentin was detected by Western blot in differentiated 3T3-L1 cells (n = 5). Differentiated 3T3-L1 cells were treated with or without compound C (CC; 10 μM) for 2 h, followed by stimulation with LPS (1 μg/mL) for 24 h. Quantitative real-time PCR analysis of (G) TNF-α, (H) omentin mRNA expression. (I) The omentin fluorescence intensity was detected by immunofluorescence (Scale bar = 20 μm) and (J) the expression of omentin protein was detected by Western blot in differentiated 3T3-L1 cells (n = 5). Differentiated 3T3-L1 cells were treated with or without amlexanox (Amx; 500 μM) for 2 h, followed by stimulation with LPS (1 μg/mL) for 24 h. Quantitative real-time PCR analysis of (K) TNF-α and (L) omentin mRNA expression in differentiated 3T3-L1 cells (n = 5). (M) The omentin fluorescence intensity was detected by immunofluorescence (n = 5). Scale bar = 20 μm. (N) The expression of omentin and (O) the ratio of *p*-AMPK to AMPK were detected by Western blot in differentiated 3T3-L1 cells (n = 5). (P) The effects of TBK1-siRNA on omentin mRNA expression were detected by quantitative real-time PCR analysis. Values are expressed as the means ± SD. One-way ANOVA was followed by the Dunnett's post hoc test. $^{\#}P < 0.05$, $^{\#\#}P < 0.01$, $^{\#\#\#}P < 0.001$ LPS vs. Control; $^{*}P < 0.05$, $^{**}P < 0.01$, $^{***}P < 0.001$ Rd + LPS or AICAR + LPS or CC + LPS or Amx + LPS vs. LPS.

induced 3T3-L1 adipocytes.

3.4. Ginsenoside Rd regulated omentin expression through the TBK1-AMPK signaling pathway in LPS-induced 3T3-L1 adipocytes

Firstly, the molecular docking results indicated that Rd could easily enter and bind the active pocket of the TBK1 protein (−10.1 kcal/mol) (Fig. 4A). Moreover, the surface plasmon resonance (SPR) technology was performed. Rd exhibited a binding affinity with protein TBK1 and the estimated equilibrium dissociation constant is 2.941 μM (Fig. 4B). Subsequently, Rd reversed the inhibitory effect of LPS on omentin mRNA, omentin protein level and fluorescence intensity. Nevertheless,

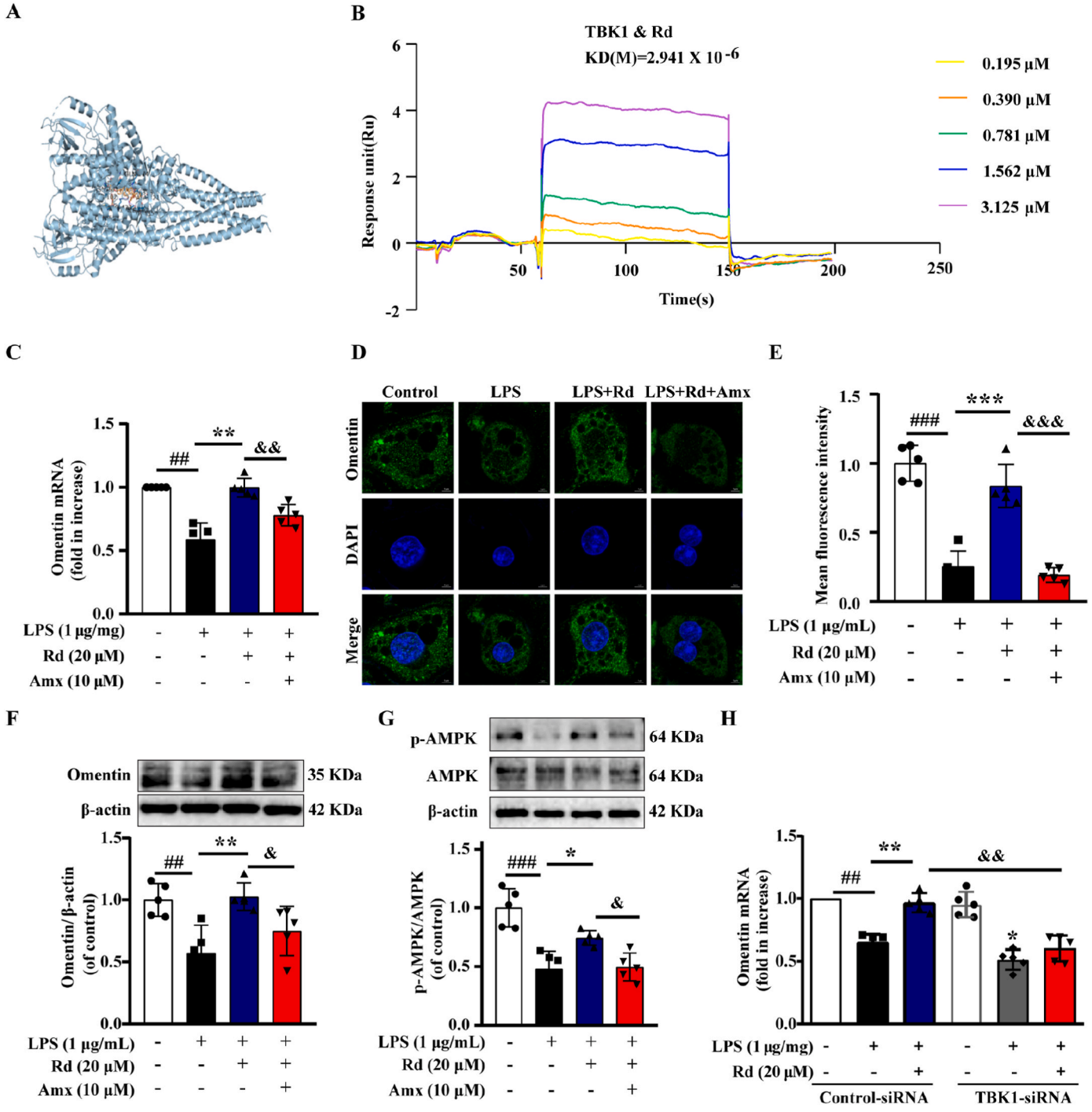

Fig. 4. Ginsenoside Rd regulated omentin expression through the TBK1-AMPK signaling pathway in LPS-induced 3T3-L1 adipocytes. (A) 3D Structure of molecular docking between Rd and the protein TBK1. (B) Surface plasmon resonance (SPR) analysis between Rd and the protein TBK1. (C) The omentin mRNA expression was measured by quantitative real-time PCR analysis in differentiated 3T3-L1 cells (n = 5). (D) The omentin fluorescence intensity was detected by immunofluorescence. (E) The statistical chart of immunofluorescence staining. Scale bar = 20 μm (n = 5). (F) The expression of omentin and (G) the ratio of *p*-AMPK to AMPK were detected by Western blot after being treated with Rd (20 μM) and Amx (500 μM) in differentiated 3T3-L1 cells. (n = 5). (H) The omentin mRNA expression was detected by quantitative real-time PCR analysis after being treated with Rd and TBK1-siRNA in differentiated 3T3-L1 cells. Values are expressed as the means ± SD. One-way ANOVA followed by the Dunnett's post hoc test. $^{\#}P < 0.05$, $^{\#\#}P < 0.01$, $^{\#\#\#}P < 0.001$ LPS vs. Control; $^{*}P < 0.05$, $^{**}P < 0.01$, $^{***}P < 0.001$ LPS + Rd vs. LPS; $^{\&}P < 0.05$, $^{\&\&}P < 0.01$, $^{\&\&\&}P < 0.001$ LPS + Rd + Amx vs. LPS + Rd or LPS + Rd + Control-siRNA vs. LPS + Rd + TBK1-siRNA.

the effects of Rd were partially abolished by the co-treatment with TBK1 inhibitor amlexanox (Fig. 4C–F). Moreover, the effect of Rd on AMPK phosphorylation was also inhibited by amlexanox (Fig. 4G). Additionally, TBK1 knockdown partially attenuated the effect of Rd on increasing the omentin expression in adipocytes (Fig. 4H). In conclusion, these data provided evidence that ginsenoside Rd could regulate omentin expression in LPS-induced adipocytes via the TBK1-AMPK signaling pathway.

3.5. Adipose tissue-specific omentin overexpression inhibited WNT5A/Ca^{2+} signaling pathway and improved mitochondrial biogenesis to ameliorate myocardial ischemia injury in HF mice

To further explore the mechanism of ginsenoside Rd in the treatment of HF, alterations of related protein content were evaluated by Western blot analysis. As shown in Fig. S7A, ISO treatment significantly increased the protein levels of WNT5A, Frizzled2 and the ratio of *p*-CAMKII to CAMKII compared with those of the control, while Rd exerted the opposite effects, which suggested that Rd could inhibit the activation of the WNT5A/Ca^{2+} signaling pathway. Next, Rd could markedly increase the expression of PGC-1α-related mitochondrial biogenic proteins, such as PGC-1α, NRF1, NRF2 and TFAM compared with the model group (Fig. S7B). In addition, the results of transmission electron microscopy showed that Rd could increase the length of mitochondria, reduce the swelling of mitochondria and restore the normal morphology of mitochondria in TAC-induced HF mice (Fig. S7C). Taken together, these results indicated that Rd promoted omentin release from adipocytes and inhibited WNT5A/Ca^{2+} signaling pathway to improve mitochondrial biogenesis.

To further verify the important role of omentin in improving HF, clinical patient samples were collected and analyzed in this study. As illustrated in Fig. 5A, the serum levels of omentin in HF patients were lower than those in healthy subjects, which demonstrated that decreased omentin levels were associated with HF. To further explore the improvement effect of omentin on HF, the adipose tissue-specific omentin overexpression was achieved by tail vein injection of AAV-omentin in CAL-induced HF mice. The results showed that adipose tissue-specific omentin overexpression significantly increased serum omentin content compared with the model group (Fig. 5B). Consistently, immunohistochemical analysis showed that adipose tissue-specific omentin overexpression increased omentin expression in sham mice and promoted omentin expression in adipose tissue of model mice (Fig. 5C and Fig. S8A). The ultrasonic electrocardiogram was used to detect the effect of omentin on cardiac function in CAL-induced HF mice. Compared with the sham group, the cardiac function was damaged as the downregulation of LV EF, LV FS and stroke volume in the model group. Conversely, adipose tissue-specific omentin overexpression improved cardiac function in HF mice (Fig. 5D–G). Additionally, adipose tissue-specific omentin overexpression significantly increased the LVPW; d, IVS; d, RWT, and LV Mass compared with the model group (Fig. 5H–K). All of these results indicated that adipose tissue-specific omentin overexpression remarkably inhibited the development of cardiac remodeling and hypertrophy. Simultaneously, HF mice appeared obviously myocardial infarct areas, and omentin significantly decreased the infarct size in HF mice (Fig. 5L and Fig. S8B). Furthermore, the histopathological examination of heart tissues in HF mice showed observable augment of left ventricular wall fibrosis, and severe morphological damage including extensive myocardial structural destruction, irregularly arranged myocardial fibers, diffusely inflammatory infiltration, and massive myocardial necrosis. Whereas, the adipose tissue-specific omentin overexpression observably ameliorated cardiac pathological features (Fig. 5M and Figs. S8C–D). As shown in Fig. 5N-O, the adipose tissue-specific omentin overexpression markedly reduced the serum BNP contents and CK activity in HF mice. These results revealed the ameliorative effect of omentin on cardiac function and myocardial ischemia injury in CAL-induced HF mice.

To further explore the mechanism of omentin in improving HF, the expression of the WNT5A/Ca^{2+} signaling pathway and mitochondrial biogenesis were investigated. The results showed that adipose tissue-specific omentin overexpression could inhibit the expression of WNT5A, Frizzled2 and decrease the ratio of *p*-CAMKII to CAMKII (Fig. 5P). By contrast, the expression of PGC-1α-related mitochondrial biogenic proteins, such as PGC-1α, NRF1, NRF2 and TFAM proteins were activated by the adipose tissue-specific omentin overexpression compared with the model group (Fig. 5Q). These data indicated that adipose tissue-specific omentin overexpression could significantly inhibit the WNT5A/Ca^{2+} signaling pathway and improve mitochondrial biogenesis to ameliorate myocardial ischemia injury in CAL-induced HF mice.

3.6. Exogenous omentin inhibited WNT5A/Ca^{2+} signaling pathway and improved mitochondrial biogenesis to ameliorate OGD-induced cardiomyocytes injury

To determine whether omentin inhibited OGD-induced cardiomyocyte injury by preventing mitochondrial damage, the mtROS and ΔψM were detected. The results showed that exogenous omentin (300 ng/mL) treatment reduced the mtROS levels (Fig. 6A, Fig. S9A and Figs. S9C and E) and restored the ΔψM (Fig. 6B, Fig. S9B and Figs. S9D and F) in OGD-induced primary neonatal rat ventricular myocytes (NRVMs) and H9c2 cells, which suggested that omentin could improve mitochondrial dysfunction. In addition, the expression of WNT5A and Frizzled2 proteins were down-regulated and the ratio of *p*-CAMKII to CAMKII was decreased after omentin treatment (Fig. 6C). Meanwhile, omentin alleviated the calcium ions in OGD-induced H9c2 cells and NRVMs, assessed by immunofluorescence staining (Fig. 6D and Figs. S9G–H), supporting that exogenous omentin could inhibit the WNT5A/Ca^{2+} signaling pathway and reduce calcium content to improve myocardial mitochondrial dysfunction. Additionally, omentin inhibited MPTP opening in OGD-induced NRVMs (Fig. 6E and Fig. S9I). Since omentin inhibited calcium production, further consideration should be given to the role of omentin in regulating mitochondrial biogenesis.

Further results showed that omentin could largely increase the expression of PGC-1α, NRF1, NRF2 and TFAM proteins compared with the OGD-induced cardiomyocytes (Fig. 6F). In addition, hypoxia-induced mitochondrial respiratory function was evaluated by seahorse analysis. The results showed that omentin could increase the values of stressed OCR and baseline OCR (Fig. 6G–I). And the ECAR value was decreased in $CoCl_2$-induced cardiomyocytes after treated with omentin (Fig. 6J-L). These results suggested that omentin could ameliorate hypoxia-induced mitochondrial respiratory disorders. Meanwhile, omentin markedly increased the ATP level, restored the mtDNA content and mitochondrial number (Fig. 6M − O), which indicated that omentin restored the decline in mitochondrial productivity caused by mitochondrial biogenesis damage. Together, these results reproduced the findings *in vitro* and confirmed that exogenous omentin could inhibit the WNT5A/Ca^{2+} signaling pathway and improve mitochondrial biogenesis to ameliorate cardiomyocytes injury.

3.7. WNT5A mediated the cardioprotective effect of omentin by regulating mitochondrial biogenesis

In the next experiment, we explored whether WNT5A mediated the cardioprotective effect of omentin to improve mitochondrial biogenesis. As shown in Fig. S10A, siRNA-mediated knockdown of the WNT5A gene was successfully conducted with an inhibition efficacy larger than 50%. Simultaneously, WNT5A knockdown could reduce mtROS production and restore ΔψM in OGD-induced H9c2 cells. And also, mitochondrial function recovery was further enhanced after treatment with omentin in WNT5A-siRNA plus OGD-induced H9c2 cells without statistically significant (Fig. 7A and B and Figs. S10B–C). In addition, WNT5A knockdown significantly reduced the protein expression of WNT5A and Frizzled2, but elevated the protein content of PGC-1α (Fig. 7C).

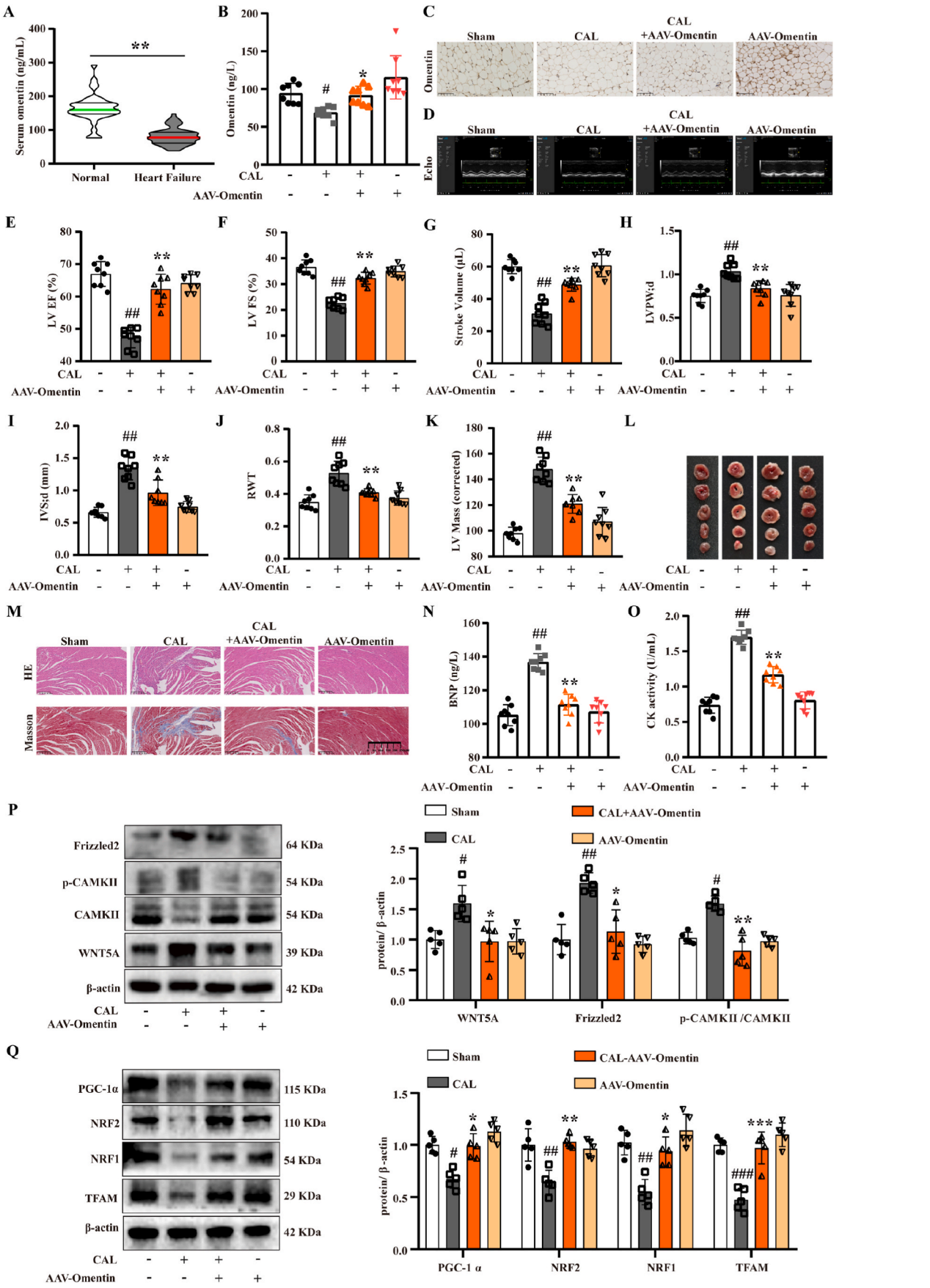

(caption on next page)

Fig. 5. Adipose tissue-specific omentin overexpression inhibited WNT5A/Ca^{2+} signaling pathway and improved mitochondrial biogenesis to ameliorate myocardial injury in HF mice. (A) Serum omentin level of HF patients and healthy subjects. A total of 58 HF patients and 38 healthy subjects were enrolled. (B) The omentin serum content of adipose tissue-specific omentin overexpression by intravenous injection of AAV-omentin and negative control by intravenous injection of AAV-NC (n = 8). (C) The expression of omentin in the inguinal fat of mice with adipose tissue-specific omentin overexpression was detected by immunohistochemistry (n = 4). Scale bar = 200 μm. (D) Representative echocardiographs of mice with AAV-omentin overexpression and the statistical results of (E) LV EF, (F) LV FS, (G) stroke volume, (H) LVPW; d, (I) IVS; d, (J) RWT and (K) LV Mass were presented (n = 8). (L) Representative TTC staining images of heart tissues of mice with AAV-omentin overexpression (n = 6). (M) Representative images of H&E and Masson staining of heart tissues of mice with AAV-omentin overexpression (n = 3), scale bar = 250 μm. (N) The serum content of BNP in mice with AAV-omentin overexpression (n = 8). (O) The serum CK activity in mice with AVV-omentin overexpression (n = 8). (P) The protein expression level of WNT5A, Frizzled2 and *p*-CAMKII/CAMKII were determined by Western blot. β-actin was used as a loading control (n = 5). (Q) The protein expression level of PGC-1α, NRF1, NRF2 and TFAM were determined by Western blot in mice with AAV-omentin overexpression. β-actin was used as a loading control (n = 5). Values are expressed as the means ± SD. (A) Unpaired Student's two-tailed *t*-test; (B–Q) One-way ANOVA followed by the Dunnett's post hoc test. $^{\#}P < 0.05$, $^{\#\#}P < 0.01$, $^{\#\#\#}P < 0.001$ vs. Sham; $^{*}P < 0.05$, $^{**}P < 0.01$, $^{***}P < 0.001$ vs. CAL.

Meanwhile, WNT5A-siRNA markedly suppressed calcium overload (Fig. 7D and Fig. S10D), increased the ATP level, restored the mtDNA content and mitochondrial number (Fig. 7E–G). Interestingly, the effect of WNT5A knockdown partially eliminated the protective effect of omentin on cardiomyocytes, which indicated that inhibition of WNT5A was largely responsible for omentin in improving mitochondrial biogenesis dysfunction.

4. Discussion

In recent decades, the aging of populations worldwide has gradually shifted the global burden of diseases such as HF [27]. It is particularly important to explore HF's pathological mechanism and treatment strategies. In this study, TAC, CAL and ISO-induced HF mice models were performed to simulate clinical symptoms of HF [28,29]. Ginsenoside Rd has been studied to reduce insulin resistance and alleviate TAC-induced cardiac hypertrophy [30,31]. In the present study, ginsenoside Rd was found to ameliorate myocardial ischemia injury in TAC, CAL and ISO-induced HF, mainly due to enhancing myocardial contractility and inhibiting cardiac pathological changes.

The interaction between the heart and adipose tissue may serve as a new perspective for the prevention and treatment of HF [3]. Many adipokines are involved in the treatment of cardiovascular diseases. Omentin is a novel adiponectin secreted mainly from visceral adipose tissue. Clinically, serum omentin level was independently associated with the prevalence of coronary heart disease [32]. Meanwhile, previous research has shown that omentin could reduce atherosclerosis by restraining the inflammatory response of macrophages [33]. In addition, our previous studies have found that Rd is one of the main components in *Panax ginseng* CA Mey and can be distributed in adipose tissue [15]. In the present study, ginsenoside Rd was found to promote the release of omentin in serum and EAT of HF mice. Furthermore, CM of isolated EAT treated with Rd could restore the viability of OGD-induced cardiomyocytes injury. Thus, Rd had the potential to regulate the crosstalk between adipose tissue and myocardial tissue to improve HF. Due to its simplicity and efficiency, LPS has been widely used to induce acute inflammatory responses in different organs [34,35]. The present study found that LPS induced significant inflammation in 3T3-L1 adipocytes. It was also verified that ginsenoside Rd could improve adipocytes inflammation induced by LPS. Consistently, Rd increased the expression of omentin in 3T3-L1 adipocytes. Moreover, the luciferase activity of omentin was increased upon the treatment with Rd. To fully understand the role of Rd in reducing adipose tissue inflammation, high-fat diet-induced and genetically obese mouse models should be recruited in the future.

AMPK is a serine/threonine-protein kinase that activates and produces ATP to promote energy metabolism. In addition, AMPK, as a central regulator of multiple metabolic pathways, has important therapeutic implications for adipocyte inflammation [36]. Activation of AMPK increases the release of adiponectin from 3T3-L1 preadipocytes to reduce inflammation in HFD-induced obese mice [37]. Furthermore, TBK1 also plays a crucial role in regulating inflammation and energy metabolism in adipose tissue. And the TBK1-AMPK axis also exerts an anti-inflammatory role in immune cells [38]. In the present study, Rd could increase TBK1 phosphorylation and AMPK phosphorylation. Moreover, AMPK agonists inhibited adipocyte inflammation and promoted the expression of omentin in adipocytes. Conversely, AMPK inhibitors aggravated inflammatory injury of adipocytes and inhibited the expression of omentin. And also, TBK1 inhibitors aggravated the inflammation of adipocytes and inhibited the expression of omentin. Meanwhile, it also inhibited the activation of AMPK phosphorylation. Thus, the TBK1-AMPK signaling pathway could regulate the expression of omentin in adipocytes. To further clarify the regulation of Rd on the TBK1-AMPK signaling pathway, virtual docking was firstly performed on Autodock Vina. Interestingly, the small molecule ligands of the ginsenoside Rd could easily enter and bind to the active pocket of the TBK1 receptor protein. And the SPR analysis also confirmed that Rd had a certain binding ability with TBK1. At the same time, the co-treatment of TBK1 inhibitors or TBK1 knockdown partially abolished the effect of Rd on increasing the ratio of *p*-AMPK to AMPK and the expression of omentin in adipocytes. Thus, TBK1 was a critical protein that Rd regulated the expression of omentin in adipocytes. To fully demonstrate the role of TBK1 in the regulation of omentin expression in adipocytes by ginsenoside Rd, adipose-specific TBK1 knockout mice should be constructed in the future.

In this study, Rd not only promoted the release of omentin in serum but also up-regulated the expression of mitochondrial biogenesis-associated proteins in HF mice. Besides, ginsenoside Rd could improve the number and morphology of myocardial mitochondria in TAC-induced HF mice. Thus, Rd might activate mitochondrial biogenesis in the myocardium of HF mice via promoting the release of omentin from adipocytes. Omentin, an adipokine expressed in adipose tissue and released into the bloodstream, was found to provide a certain therapeutic effect on complex diseases such as osteoporosis, acute lung injury, arterial calcification, and MI/R injury [39–41]. In addition, clinical studies have found that decreased serum omentin levels are associated with the degree of heart damage, and serum omentin levels can be a marker of risk for HF patients [42]. Whereas, the improvement of omentin on HF is not yet clear, and its potential mechanism still needs to be further elucidated. In the present study, the serum omentin level was down-regulated in HF patients compared with healthy subjects clinically. Additionally, omentin could ameliorate acute myocardial injury in myocardial ischemia/reperfusion mice [6]. In our present research, increased circulating omentin level via adipose tissue-specific omentin overexpression observably ameliorated cardiac function, myocardial infarct size and cardiac pathological features in HF mice. Mitochondria play a vital role in the pathogenesis of heart diseases, and mitochondrial-targeted therapy provides a direction to treat heart diseases [43–45]. Mitochondria are the primary source of ROS. After myocardial ischemia, the mitochondrial oxidative respiratory chain produces ROS, and the ROS level imbalance initiates the opening of MPTP [46]. Moreover, omentin could inhibit DOX-induced cardiac apoptosis by reducing mitochondrial ROS production [47]. At present, exogenous omentin treatment reduced mtROS levels and restored ΔψM to attenuate OGD-induced cardiomyocyte injury. Meanwhile, mitochondrial biogenesis is the process of mitochondrial growth and

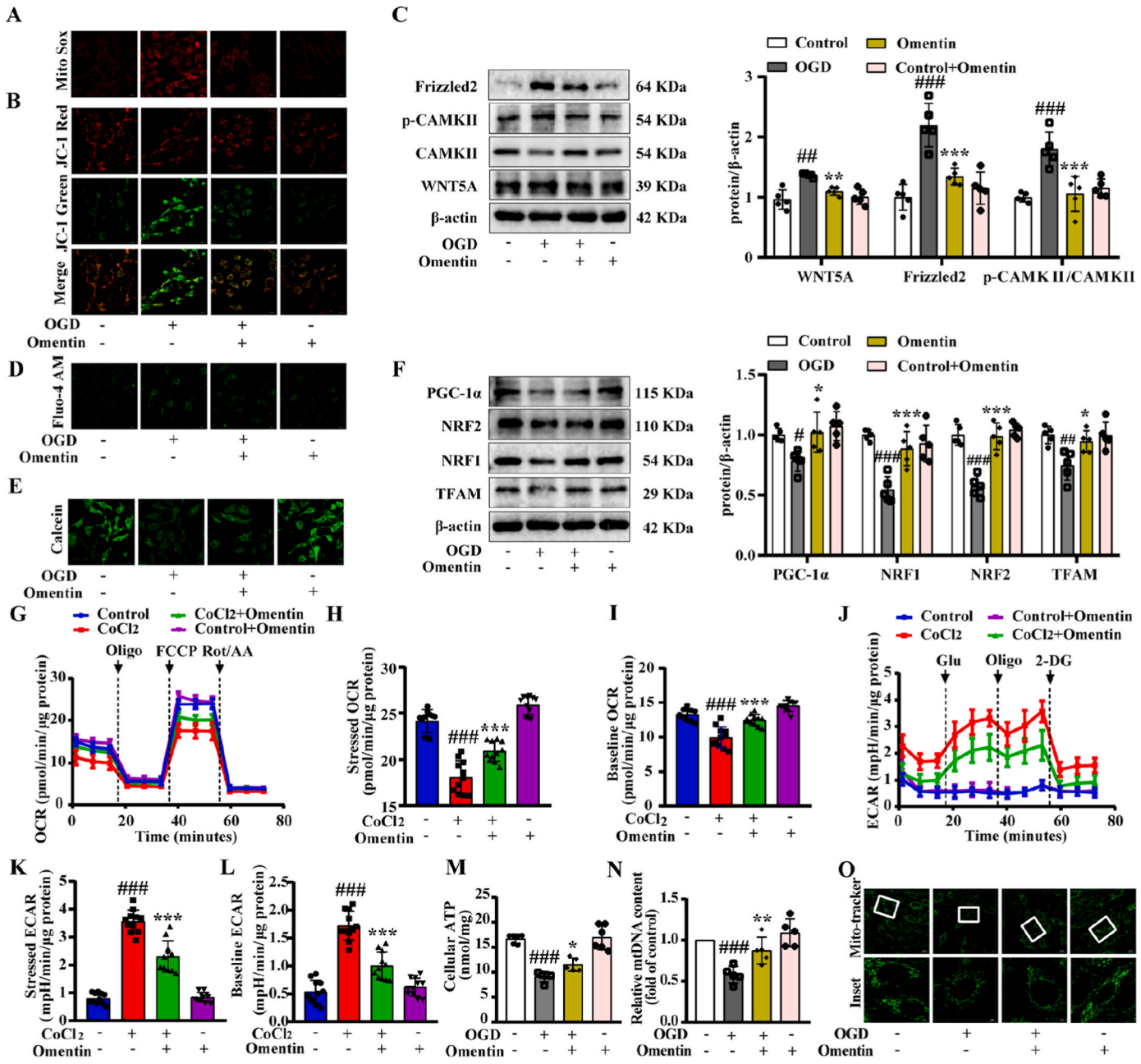

Fig. 6. Exogenous omentin inhibited WNT5A/Ca^{2+} signaling pathway and improved mitochondrial biogenesis to ameliorate OGD-induced cardiomyocyte injury. (A) The mtROS level was determined by MitoSOX in NRVMs. Scale bar = 20 μm (n = 5). (B) The mitochondrial membrane potential was measured by JC-1 staining in NRVMs. Scale bar = 20 μm (n = 5). (C) The protein expression level of WNT5A, Frizzled2 and *p*-CAMKII/CAMKII were determined by Western blot. β-actin was used as a loading control (n = 5). (D) Calcium ion fluorescence content was detected by Fluo-4 AM in NRVMs. Scale bar = 20 μm (n = 5). (E) MPTP opening was detected by MPTP Assay Kit in NRVMs (n = 5). (F) The protein expression levels of PGC-1α, NRF1, NRF2 and TFAM were determined by Western blot. β-actin was used as a loading control (n = 5). (G–I) Oxygen consumption rate (OCR) was measured in $CoCl_2$-induced cardiomyocytes (n = 5). (J–L) Extracellular acidification rate (ECAR) was measured in $CoCl_2$-induced cardiomyocytes (n = 5). (M) The level of ATP was tested by ATP Assay Kit (n = 5). (N) MtDNA content was detected by PCR (n = 5). (O) The number of mitochondria was measured by Mito-tracker fluorescence intensity. Scale bar = 20 μm (n = 5). Values are expressed as the means ± SD. One-way ANOVA was followed by the Dunnett's post hoc test. $^{\#}P < 0.05$, $^{\#\#}P < 0.01$, $^{\#\#\#}P < 0.001$ OGD vs. Control; $^{*}P < 0.05$, $^{**}P < 0.01$, $^{***}P < 0.001$ OGD + omentin vs. OGD.

reproduction, and also affects mitochondrial energy metabolism. PGC-1α is a co-regulatory transcriptional factor that induces mitochondrial biogenesis and regulates energy metabolism through activating different transcription factors, including NRF1 and NRF2, followed by activation of TFAM and driving transcription and replication of mitochondrial DNA [11,48,49]. In the present study, AAV-omentin overexpression reversed the down-regulation of protein levels of PGC-1α, NRF1, NRF2 and TFAM in HF mice. Consistently, the exogenous omentin treatment promoted mitochondrial biogenesis *in vitro*. On the other hand, the ultrastructure of cardiomyocytes is mainly powered by mitochondrial ATP production. The complex system composed of mtDNA encoded by the mitochondrial nuclear genome and energy metabolism mechanism is necessary to coordinate and control cardiac mitochondrial biogenesis [50]. The present study found that exogenous omentin markedly increased the ATP level, restored the mtDNA content and mitochondrial number. These evidences also

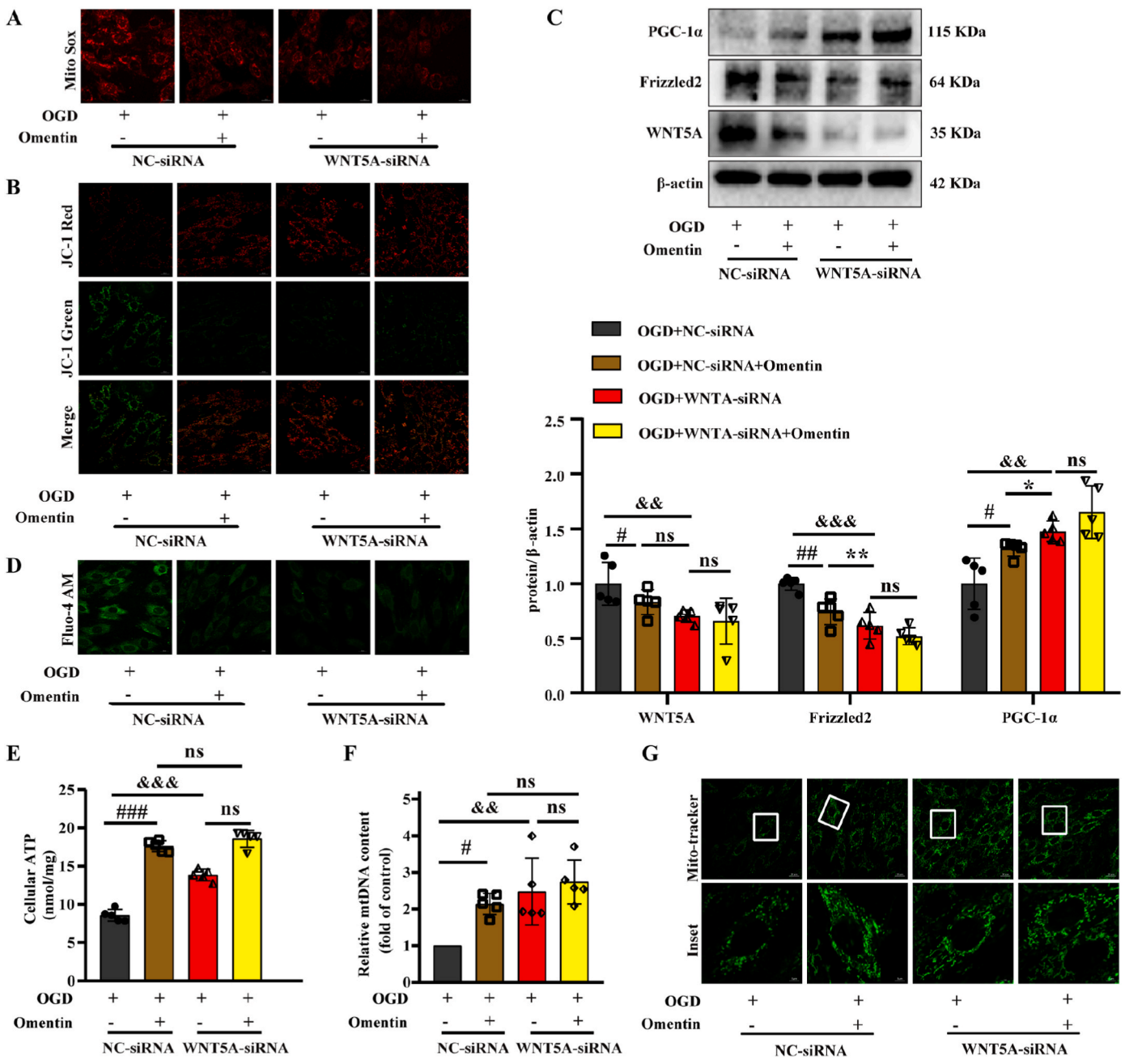

Fig. 7. WNT5A mediated the cardioprotective effect of omentin by regulating mitochondrial biogenesis. (A) The mtROS level was determined by MitoSOX in cardiomyocytes. Scale bar = 20 μm (n = 5). (B) Mitochondrial membrane potential was measured by JC-1 staining. Scale bar = 20 μm (n = 5). (C) The protein expression of WNT5A, Frizzled2 and PGC-1α were determined by Western blot. β-actin was used as a loading control (n = 5). (D) Calcium ion content was detected by Fluo-4 AM. Scale bar = 20 μm (n = 5). (E) The level of ATP was tested by ATP Assay Kit in cardiomyocytes (n = 5). (F) MtDNA content was detected by PCR. (G) The number of mitochondria was measured by Mito-tracker fluorescence intensity. Scale bar = 20 μm (n = 5). Values are expressed as the means ± SD. One-way ANOVA followed by the Dunnett's post hoc test. $^{\#}P < 0.05$, $^{\#\#}P < 0.01$, $^{\#\#\#}P < 0.001$ OGD + NC-siRNA + Omentin vs. OGD + NC-siRNA; $^{*}P < 0.05$, $^{**}P < 0.01$, $^{***}P < 0.001$ OGD + WNT5A-siRNA vs. OGD + NC-siRNA + Omentin; $^{\&}P < 0.05$, $^{\&\&}P < 0.01$, $^{\&\&\&}P < 0.001$ OGD + WNT5A-siRNA vs. OGD + NC-siRNA. NS = no significance.

suggested that omentin could regulate energy metabolism and improve myocardial injury via promoting mitochondrial biogenesis.

Mitochondrial Ca^{2+} overload can induce MPTP opening and mitochondrial swelling, decrease ATP synthesis, increase reactive oxygen species (ROS) production, and lead to mitochondrial damage and cardiac remodeling, and eventually develop into HF [51]. In addition, Ca^{2+} overload is one of the main causes of mitochondrial biogenesis disorder in cardiomyocytes [52]. Clinical studies have shown that WNT5A levels in the serum and myocardium of patients with HF are higher than normal. It also promotes myocardial inflammation and fibrosis [53,54]. WNT5A is enhanced by binding to the Frizzled2 receptor, promoting intracellular calcium release and activating Ca^{2+}/calmodulin-dependent protein kinase II (CAMKII) in a G-protein-dependent manner after myocardial ischemia-reperfusion [55]. Moreover, secreted frizzled-related protein 5 (SFRP5) is not only an adipokine, but also an endogenous inhibitor of WNT5A, which inhibits the WNT5A/Ca^{2+} signaling pathway to treat obesity and type 2 diabetes [56]. In the present study, adipose tissue-specific omentin overexpression down-regulated the protein expression of WNT5A, Frizzled2 and the ratio of *p*-CAMKII to CAMKII in HF mice. Consistently,

exogenous omentin inhibited the WNT5A/Ca^{2+} signaling pathway, decreased calcium fluorescence intensity and inhibited MPTP opening in OGD-induced H9c2 cells and NRVMs. These evidences further suggested that omentin improved myocardial injury by inhibiting the WNT5A/Ca^{2+} signaling pathway *in vivo* and *in vitro*. Nevertheless, whether the inhibition of the WNT5A/Ca^{2+} signaling pathway was the primary cause of omentin's improvement in mitochondrial biogenesis remained to be further elucidated. Therefore, further WNT5A knockdown by siRNA was conducted *in vitro*. The results found that inhibition of WNT5A reduced mtROS levels, restored ΔψM and up-regulated the expression of PGC-1α. Moreover, WNT5A knockdown increased the ATP level, restored the mtDNA content and mitochondrial number. However, the protective effect of omentin on mitochondrial function was partially eliminated by WNT5A knockdown. It revealed that WNT5A was primarily responsible for omentin in improving mitochondrial biogenesis dysfunction. Thus, omentin could promote mitochondrial biogenesis and improve HF through inhibition of WNT5A/Ca^{2+} signaling pathway and calcium ion release. In addition, Rd inhibited the up-regulation levels of WNT5A, Frizzled2 and the ratio of *p*-CAMKII to CAMKII in HF mice. Herein, these results suggested that Rd promoted omentin release from adipocytes and inhibited the WNT5A/Ca^{2+} signaling pathway to improve mitochondrial biogenesis function to ameliorate myocardial ischemia injury.

5. Conclusions

Overall, Rd, one of the active components in ginseng, regulates the TBK1-AMPK signaling pathway to promote the release of omentin from adipocytes. Moreover, the increased release of omentin could ameliorate myocardial ischemia injury by improving mitochondrial biogenesis function through inhibition of WNT5A/Ca^{2+} signaling pathway. Thus, Rd could modulate the crosstalk between adipocytes and cardiomyocytes to ameliorate myocardial ischemia injury (the diagrammatic summary is shown in Fig. 8), which not only proposed novel mechanistic insights but also identified Rd as a potential drug candidate for HF treatment.

Author contributions

The study was conceived and planned by Fang Li, Junping Kou, Fuming Liu and Boyang Yu. The manuscript was written and revised by Shiyao Wan and Fang Li. Shiyao Wan, Zekun Cui, Lingling Wu and Tao Liu participated in the experiment design, collection and analysis of data results. The partial experiments were performed by Zekun Cui, Lingling Wu, Fan Zhang, Jingui Hu and Jiangwei Tian. All other authors approved the manuscript prior to submission. All authors have seen the manuscript and approved to submit to your journal.

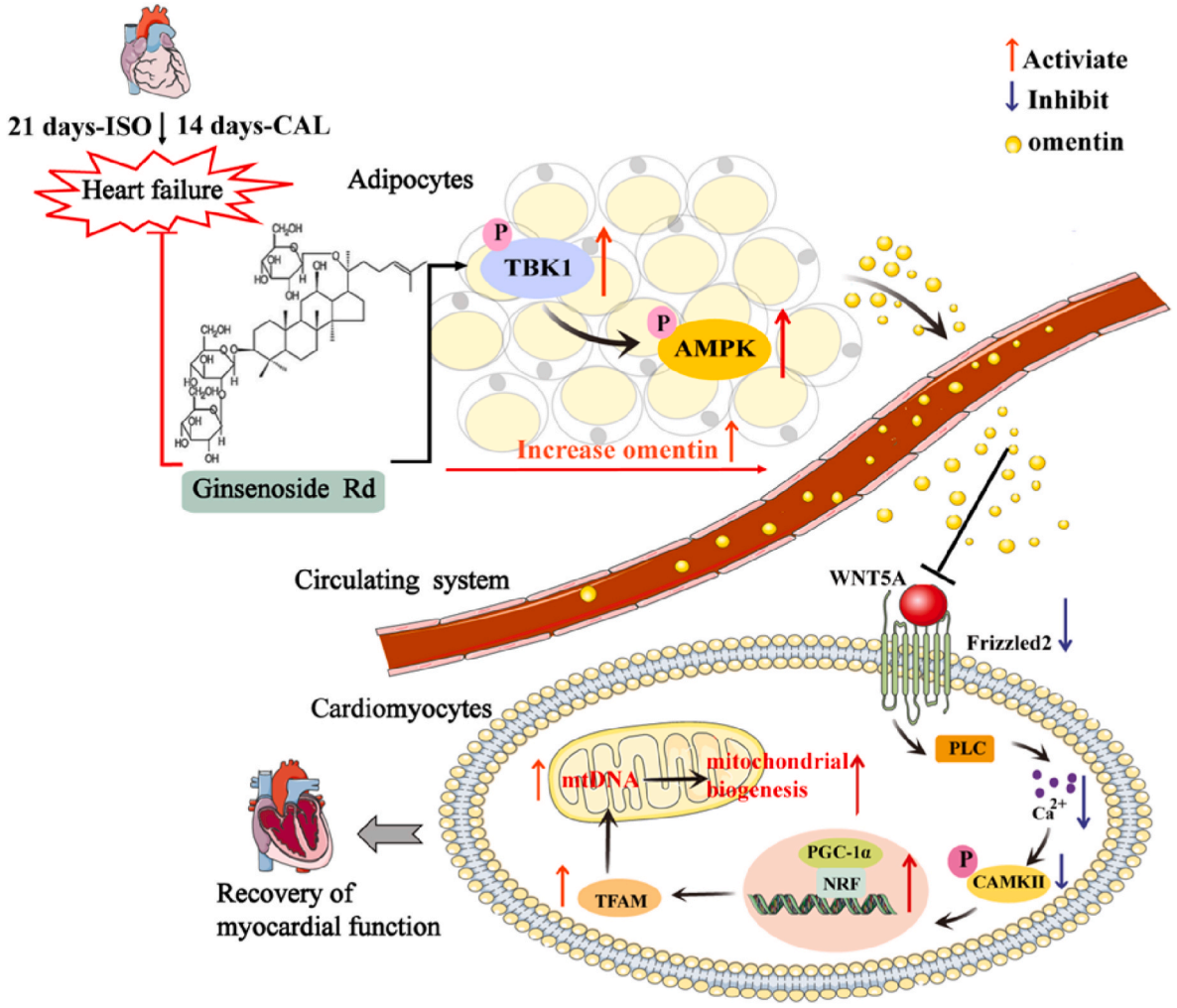

Fig. 8. Schematic diagram of the regulatory mechanism of ginsenoside Rd on heart failure. Rd regulated the TBK1-AMPK signaling pathway to promote the release of omentin from adipocytes. Moreover, the increased release of omentin could ameliorate myocardial ischemia injury by improving mitochondrial biogenesis function through inhibiting WNT5A/Ca^{2+} signaling pathway. Thus, Rd modulated the crosstalk between adipocytes and cardiomyocytes to ameliorate HF.

Declaration of competing interest

The authors declare no conflicts of interest.

Acknowledgments

Financial support by the National Science Foundation of China (No. 81973506, No. 82274231), Young Talent Support Project of Jiangsu Association for Science and Technology (TJ-2022-025) and Qinglan Project of Jiangsu Province are gratefully acknowledged.

Appendix A. Supplementary data

Supplementary data to this article can be found online at https://doi.org/10.1016/j.redox.2023.102610.

References

[1] P. Ponikowski, A.A. Voors, S.D. Anker, et al., ESC Guidelines for the diagnosis and treatment of acute and chronic heart failure [J], Rev. Esp. Cardiol. 69 (12) (2016) 1167, https://doi.org/10.1016/j.rec.2016.11.005, 2016.
[2] T.H.K. Teng, J. Hung, M. Knuiman, et al., Trends in long-term cardiovascular mortality and morbidity in men and women with heart failure of ischemic versus non-ischemic aetiology in Western Australia between 1990 and 2005 [J], Int. J. Cardiol. 158 (3) (2012) 405–410, https://doi.org/10.1016/j.ijcard.2011.01.061.
[3] H.M. Christensen, C. Kistorp, M. Schou, et al., Cross-talk between the heart and adipose tissue in cachectic heart failure patients with respect to alterations in body composition: a prospective study [J], Metabolism 63 (1) (2014) 141–149, https://doi.org/10.1016/j.metabol.2013.09.017.
[4] Y. Nakamura, S. Kita, Y. Tanaka, et al., Adiponectin stimulates exosome release to enhance mesenchymal stem-cell-driven therapy of heart failure in mice [J], Mol. Ther. 28 (10) (2020) 2203–2219, https://doi.org/10.1016/j.ymthe.2020.06.026.
[5] S. Zhao, C.M. Kusminski, P.E. Scherer, Adiponectin, leptin and cardiovascular disorders [J], Circ. Res. 128 (1) (2021) 136–149, https://doi.org/10.1161/CIRCRESAHA.120.314458.
[6] Y. Kataoka, R. Shibata, K. Ohashi, et al., Omentin prevents myocardial ischemic injury through AMP-activated protein kinase- and Akt-dependent mechanisms [J], J. Am. Coll. Cardiol. 63 (24) (2014) 2722–2733, https://doi.org/10.1016/j.jacc.2014.03.032.
[7] S.M. Reilly, S.-H. Chiang, S.J. Decker, et al., An inhibitor of the protein kinases TBK1 and IKK-ε improves obesity-related metabolic dysfunctions in mice [J], Nat. Med. 19 (3) (2013) 313–321, https://doi.org/10.1038/nm.3082.
[8] P. Zhao, K.I. Wong, X. Sun, et al., TBK1 at the crossroads of Inflammation and energy homeostasis in adipose tissue [J], Cell 172 (4) (2018) 731–743, https://doi.org/10.1016/j.cell.2018.01.007, e712.
[9] M.P. Murphy, R.C. Hartley, Mitochondria as a therapeutic target for common pathologies [J], Nat. Ev. Drug. Discov. 17 (12) (2018) 865–886, https://doi.org/10.1038/nrd.2018.174.
[10] G.W. Dorn, R.B. Vega, D.P. Kelly, Mitochondrial biogenesis and dynamics in the developing and diseased heart [J], Genes Dev. 29 (19) (2015) 1981–1991, https://doi.org/10.1101/gad.269894.115.
[11] Y. Li, Y. Feng, X. Liu, et al., Songorine promotes cardiac mitochondrial biogenesis via Nrf2 induction during sepsis [J], Redox. Biol. 38 (2021), 101771, https://doi.org/10.1016/j.redox.2020.101771.
[12] X. Wu, S. Zhou, N. Zhu, et al., Resveratrol attenuates hypoxia/reoxygenation-induced Ca^{2+} overload by inhibiting the Wnt5a/Frizzled-2 pathway in rat H9c2 cells [J], Mol. Med. Rep. 10 (5) (2014) 2542–2548, https://doi.org/10.3892/mmr.2014.2488.
[13] W. Fan, Y. Huang, H. Zheng, et al., Ginsenosides for the treatment of metabolic syndrome and cardiovascular diseases: pharmacology and mechanisms, J. Biomed. Pharmacother. 132 (2020), 110915, https://doi.org/10.1016/j.biopha.2020.110915.
[14] N. Zhang, X. An, P. Lang, et al., Ginsenoside Rd contributes the attenuation of cardiac hypertrophy in vivo and in vitro [J], Biomed. Pharmacother. 109 (2019) 1016–1023, https://doi.org/10.1016/j.biopha.2018.10.081.
[15] F. Li, L. Pang, L. Zhang, et al., YiQiFuMai powder injection ameliorates chronic heart failure through cross-talk between adipose tissue and cardiomyocytes via up-regulation of circulating adipokine omentin [J], Biomed. Pharmacother. 119 (2019), 109418, https://doi.org/10.1016/j.biopha.2019.109418.
[16] C. Kilkenny, W. Browne, I.C. Cuthill, et al., Animal research: reporting in vivo experiments: the ARRIVE guidelines [J], Br. J. Pharmacol. 160 (7) (2010) 1577–1579, https://doi.org/10.1111/j.1476-5381.2010.00872x.
[17] J.C. Mcgrath, E.M. Mclachlan, R. Zeller, Transparency in research involving animals: the basel declaration and new principles for reporting research in BJP manuscripts [J], Br. J. Pharmacol. 172 (10) (2015) 2427–2432, https://doi.org/10.1111/bph.12956.
[18] N. Percie Du Sert, V. Hurst, A. Ahluwalia, et al., The ARRIVE guidelines 2.0: updated guidelines for reporting animal research [J], PloS. Biol. 18 (7) (2020), e3000410, https://doi.org/10.1371/journal.pbio.3000410.
[19] Q.Q. Chen, G. Ma, J.F. Liu, et al., Neuraminidase 1 is a driver of experimental cardiac hypertrophy [J], Eur. Heart J. 42 (36) (2021) 3770–3782, https://doi.org/10.1093/eurheartj/ehab347.
[20] A.H. Maass, M. Buvoli, Cardiomyocyte preparation, culture, and gene transfer [J], Methods Mol. Biol. 366 (2007) 321–330, https://doi.org/10.1007/978-1-59745-030-0_18.
[21] Q. Lai, G.Y. Yuan, H. Wang, et al., Exploring the protective effects of schizandrol A in acute myocardial ischemia mice by comprehensive metabolomics profiling integrated with molecular mechanism studies [J], Acta Pharmacol. Sin. 41 (8) (2020) 1058–1072, https://doi.org/10.1038/s41401-020-0377-7.
[22] F. Li, X. Fan, Y. Zhang, et al., Cardioprotection by combination of three compounds from ShengMai preparations in mice with myocardial ischemia/reperfusion injury through AMPK activation-mediated mitochondrial fission [J], Sci. Rep. 6 (2016), 37114, https://doi.org/10.1038/srep37114.
[23] O. Gjesdal, D.A. Bluemke, J.A. Lima, Cardiac remodeling at the population level–risk factors, screening, and outcomes [J], Nat. Rev. Cardiol. 8 (12) (2011) 673–685, https://doi.org/10.1038/nrcardio.2011.154.
[24] S. Gong, J. Liu, S. Wan, et al., Schisandrol A attenuates myocardial ischemia/reperfusion-induced myocardial apoptosis through upregulation of 14-3-3 [J], Oxid. Med. Cell. Longev. 2021 (2021), 5541753, https://doi.org/10.1155/2021/5541753.
[25] R. Bai, C. Yuan, W. Sun, et al., NEK2 plays an active role in tumorigenesis and tumor microenvironment in non-small cell lung cancer [J], Int. J. Biol. Sci. 17 (8) (2021) 1995–2008, https://doi.org/10.7150/ijbs.59019.
[26] Q.D. Xia, Y. Xun, J.L. Lu, et al., Network pharmacology and molecular docking analyses on Lianhua Qingwen capsule indicate Akt1 is a potential target to treat and prevent COVID-19 [J], Cell Prolif 53 (12) (2020), e12949, https://doi.org/10.1111/cpr.12949.
[27] J. Spencer, A. Degu, K. Hassen Abate, et al., Global, regional, and national incidence, prevalence, and years lived with disability for 354 diseases and injuries for 195 countries and territories, 1990-2017: a systematic analysis for the Global Burden of Disease Study 2017 [J], Lancet (London, England) 392 (10159) (2018) 1789–1858, https://doi.org/10.1016/S0140-6736(18)32279-7.
[28] D. Grimm, D. Elsner, H. Schunkert, et al., Development of heart failure following isoproterenol administration in the rat: role of the renin-angiotensin system [J], Cardiovasc. Res. 37 (1) (1998) 91.
[29] F. Keihanian, M. Moohebati, A. Saeidinia, et al., Therapeutic effects of medicinal plants on isoproterenol-induced heart failure in rats [J], Biomed. Pharmacother. 134 (2021), 111101, https://doi.org/10.1016/j.biopha.2020.111101.
[30] L. Yao, Z. Han, G. Zhao, et al., Ginsenoside Rd ameliorates high fat diet-induced obesity by enhancing adaptive thermogenesis in a cAMP-dependent manner [J], Obesity 28 (4) (2020) 783–792, https://doi.org/10.1002/oby.22761.
[31] C. Zhang, X. Liu, H. Xu, et al., Protopanaxadiol ginsenoside Rd protects against NMDA receptor-mediated excitotoxicity by attenuating calcineurin-regulated DAPK1 activity [J], Sci. Rep. 10 (1) (2020) 8078, https://doi.org/10.1038/s41598-020-64738-2.
[32] X. Zhong, H.Y. Zhang, H. Tan, et al., Association of serum omentin-1 levels with coronary artery disease [J], Acta Pharmacol. Sin. 32 (7) (2011) 873–878, https://doi.org/10.1038/aps.2011.26.
[33] M. Hiramatsu-Ito, R. Shibata, K. Ohashi, et al., Omentin attenuates atherosclerotic lesion formation in apolipoprotein E-deficient mice [J], Cardiovasc. Res. 110 (1) (2016) 107–117, https://doi.org/10.1093/cvr/cvv282.
[34] L.G. Hersoug, P. Møller, S. Loft, Role of microbiota-derived lipopolysaccharide in adipose tissue inflammation, adipocyte size and pyroptosis during obesity [J], Nutr. Res. Rev. 31 (2) (2018) 153–163, https://doi.org/10.1017/S0954422417000269.
[35] T.W. Jung, H.S. Park, G.H. Choi, et al., β-aminoisobutyric acid attenuates LPS-induced inflammation and insulin resistance in adipocytes through AMPK-mediated pathway [J], J. Biomed. Sci. 25 (1) (2018) 27, https://doi.org/10.1186/s12929-018-0431-7.
[36] E.A. Day, R.J. Ford, G.R. Steinberg, AMPK as a therapeutic target for treating metabolic diseases [J], Trends Endocrinol. Metabol. 28 (8) (2017) 545–560, https://doi.org/10.1016/j.tem.2017.05.004.
[37] Y.M. Kang, H.A. Kang, D.C. Cominguez, et al., Papain ameliorates lipid accumulation and inflammation in high-fat diet-induced obesity mice and 3T3-L1 adipocytes via AMPK activation [J], Int. J. Mol. Sci. 22 (18) (2021) 9885, https://doi.org/10.3390/ijms22189885.
[38] P. Zhao, A.R. Saltiel, Interaction of adipocyte metabolic and immune functions through TBK1 [J], Front. Immunol. 11 (2020), 592949, https://doi.org/10.3389/fimmu.2020.592949.
[39] S.S. Rao, Y. Hu, P.L. Xie, et al., Omentin-1 prevents inflammation-induced osteoporosis by downregulating the pro-inflammatory cytokines [J], Bone. Res. 6 (2018) 9, https://doi.org/10.1038/s41413-018-0012-0.
[40] Y. Zhou, C. Hao, C. Li, et al., Omentin-1 protects against bleomycin-induced acute lung injury [J], Mol. Immunol. 103 (2018), https://doi.org/10.1016/j.molimm.2018.09.007.
[41] F. Xu, F.X.Z. Li, X. Lin, et al., Adipose tissue-derived omentin-1 attenuates arterial calcification via AMPK/Akt signaling pathway [J], Aging 11 (20) (2019) 8760–8776, https://doi.org/10.18632/aging.102251.
[42] T. Narumi, T. Watanabe, S. Kadowaki, et al., Impact of serum omentin-1 levels on cardiac prognosis in patients with heart failure [J], Cardiovasc. Diabetol. 13 (2014) 84, https://doi.org/10.1186/1475-2840-13-84.
[43] L.A. Kiyuna, R.P.E. Albuquerque, C.-H. Chen, et al., Targeting mitochondrial dysfunction and oxidative stress in heart failure: challenges and opportunities [J], Free Radic. Biol. Med. 129 (2018) 155–168, https://doi.org/10.1016/j.freeradbiomed.2018.09.019.

[44] B. Zhou, R. Tian, Mitochondrial dysfunction in pathophysiology of heart failure [J], J. Clin. Invest. 128 (9) (2018) 3716–3726, https://doi.org/10.1172/JCI120849.
[45] G. Bisaccia, F. Ricci, S. Gallina, et al., Mitochondrial dysfunction and heart disease: critical appraisal of an overlooked association [J], Int. J. Mol. Sci. 22 (2) (2021) 614, 10.3390/ijms22020614.
[46] Y. Xin, X. Zhang, J. Li, et al., New insights into the role of mitochondria quality control in ischemic heart disease [J], Front. Cardiovasc. Med. 8 (2021), 774619, https://doi.org/10.3389/fcvm.2021.774619.
[47] K. Kazama, M. Okada, H. Yamawaki, Adipocytokine, omentin inhibits doxorubicin-induced H9c2 cardiomyoblasts apoptosis through the inhibition of mitochondrial reactive oxygen species [J], Biochem. Biophys. Res. Commun. 457 (4) (2015) 602–607, https://doi.org/10.1016/j.bbrc.2015.01.032.
[48] S. Sihag, S. Cresci, A.Y. Li, et al., PGC-1alpha and ERRalpha target gene downregulation is a signature of the failing human heart [J], J. Mol. Cell. Cardiol. 46 (2) (2009) 201–212, https://doi.org/10.1016/j.yjmcc.2008.10.025.
[49] F.R. Jornayvaz, G.I. Shulman, Regulation of mitochondrial biogenesis [J], Essays. Biochem. 47 (2010) 69–84, https://doi.org/10.1042/bse0470069.
[50] R.B. Vega, J.L. Horton, D.P. Kelly, Maintaining ancient organelles: mitochondrial biogenesis and maturation [J], Circ. Res. 116 (11) (2015) 1820–1834, https://doi.org/10.1161/CIRCRESAHA.116.305420.
[51] H.X. Xu, S.M. Cui, Y.M. Zhang, et al., Mitochondrial Ca regulation in the etiology of heart failure: physiological and pathophysiological implications [J], Acta Pharmacol. Sin. 41 (10) (2020) 1301–1309, https://doi.org/10.1038/s41401-020-0476-5.
[52] K. Bianchi, G. Vandecasteele, C. Carli, et al., Regulation of Ca^{2+} signalling and Ca^{2+}-mediated cell death by the transcriptional coactivator PGC-1alpha [J], Cell. Death. Differ. 13 (4) (2006) 586–596.
[53] C. Silva-Alvarez, M.S. Arrázola, J.A. Godoy, et al., Canonical Wnt signaling protects hippocampal neurons from Aβ oligomers: role of non-canonical Wnt-5a/Ca^{2+} in mitochondrial dynamics [J], Front. Cell. Neurosci. 7 (2013) 97, https://doi.org/10.3389/fncel.2013.00097.
[54] A. Abraityte, L.E. Vinge, E.T. Askevold, et al., Wnt5a is elevated in heart failure and affects cardiac fibroblast function [J], J. Mol. Med. (Berl.) 95 (7) (2017) 767–777, https://doi.org/10.1007/s00109-017-1529-1.
[55] S.S. Zhou, F. He, A.H. Chen, et al., Suppression of rat frizzled-2 attenuates hypoxia/reoxygenation-induced Ca^{2+} accumulation in rat H9c2 cells [J], Exp. Cell Res. 318 (13) (2012) 1480–1491, https://doi.org/10.1016/j.yexcr.2012.03.030.
[56] D. Wang, Y. Zhang, C. Shen, Research update on the association between SFRP5, an anti-inflammatory adipokine, with obesity, type 2 diabetes mellitus and coronary heart disease [J], J. Cell Mol. Med. 24 (5) (2020) 2730–2735, https://doi.org/10.1111/jcmm.15023.